Wimer, B.M. (1997). Therapeutic immunostimulating effects of plant mitogens exemplified by the L_4 isolectin of PHA. Cancer Biother. Radiopharm. 12, 195–212.

Yamada, T., Iwabuki, H., Kanno T., Tanaka, H., Kawai, T., Fukuda, H., Kondo, A., Seno, M., Tanizawa, K., and Kuroda, S. (2001). Physicochemical and immunological characterization of hepatitis B virus envelope particles exclusively consisting of the entire L (pre-S1 + pre-S2 + S) protein. Vaccine 19, 3154–3163.

Yamada, T., Iwasaki, Y., Tada, H., Iwabuki, H., Chuah, M.K., Vandendriessche, T., Fukuda, H., Kondo, A., Ueda, M., Seno, M., Tanizawa, K., and Kuroda, S. (2003). Nanoparticles for the delivery of genes and drugs to human hepatocytes. Nat. Biotechnol. 21, 885–890.

Yamashita, K., Tachibana, Y., Ohkura, T., and Kobata, K. (1985). Enzymatic basis for the structural changes of asparagine-linked sugar chains of membrane glycoproteins of baby hamster kidney cells induced by polyoma transformation. J. Biol. Chem. 260, 3693–3969.

Zurita, A.J., Arap, W., and Pasqualini, R. (2003). Mapping tumor vascular diversity by screening phage display libraries. J. Control. Release 91, 183–186.

Address reprint requests to:
Dr. Shun'ichi Kuroda
Department of Structural Molecular Biology
Institute of Scientific and Industrial Research
Osaka University
8-1 Mihogaoka
Ibaraki, Osaka 567-0047, Japan

E-mail: skuroda@sanken.osaka-u.ac.jp

Received for publication March 25, 2008; accepted after revision June 25, 2008.

Published online: August 15, 2008.

the FEBS Journal

Expression of squamous cell carcinoma antigen-1 in liver enhances the uptake of hepatitis B virus envelope-derived bio-nanocapsules in transgenic rats

Takeshi Kasuya[1,2], Shintaro Nomura[2], Takashi Matsuzaki[1,3], Joohee Jung[1,3,*], Tadanori Yamada[1], Kenji Tatematsu[1], Toshihide Okajima[1], Katsuyuki Tanizawa[1,2] and Shun'ichi Kuroda[1,3]

1 Department of Structural Molecular Biology, The Institute of Scientific and Industrial Research, Osaka University, Japan
2 Graduate School of Frontier Bioscience, Osaka University, Japan
3 Japan Science and Technology Agency, Kawaguchi, Saitama, Japan

Keywords
bio-nanocapsule; drug delivery system; hepatitis B virus; squamous cell carcinoma antigen-1; transgenic rat

Correspondence
S. Kuroda, Department of Structural Molecular Biology, The Institute of Scientific and Industrial Research, Osaka University, 8-1 Mihogaoka, Ibaraki, Osaka 567-0047, Japan
Fax: +81 6 6879 8462
Tel: +81 6 6879 8462
E-mail: skuroda@sanken.osaka-u.ac.jp

***Present address**
Institute for Innovative Cancer Research, Asan Medical Center, Seoul, Korea

(Received 22 July 2008, revised 18 September 2008, accepted 22 September 2008)

doi:10.1111/j.1742-4658.2008.06698.x

We previously developed the bio-nanocapsule, which consists of hepatitis B virus envelope L proteins. The bio-nanocapsule can be used to deliver genes and drugs specifically to the human liver-derived tissues in xenograft models, presumably by utilizing the human liver-specific mechanism of hepatitis B virus infection. The hepatitis B virus tropism is highly restricted to humans and higher primates. Thus, to evaluate the *in vivo* therapeutic effects of forthcoming bio-nanocapsule-based medicines, it will be crucial to develop an animal model whose liver is susceptible to both bio-nanocapsule and hepatitis B virus. In the present study, we aimed to establish a bio-nanocapsule-susceptible animal model using transgenic rats expressing squamous cell carcinoma antigen-1 (SCCA1), which has been proposed to be a receptor for hepatitis B virus, interacting with the hepatitis B virus envelope protein and enhancing the cellular uptake of hepatitis B virus. We show that the recombinant SCCA1 protein interacts directly with bio-nanocapsule and inhibits its attachment to the cultured human liver-derived cells. Furthermore, we have established a transgenic rat that specifically expresses SCCA1 in the liver and also demonstrate that the amount of bio-nanocapsule accumulated in the liver is significantly increased by the SCCA1 expression. Histological analysis suggests that bio-nanocapsule is preferentially incorporated into the SCCA1-expressing hepatocytes but not into macrophages, such as Küppfer cells, nor into endothelial cells. Therefore, this animal model is expected to be useful for the development of bio-nanocapsule-based medicines.

Hepatitis B virus (HBV) specifically infects the liver of humans and higher primates. The hepatophilic tropism of HBV is mainly determined by the function of the HBV envelope protein (also called HBV surface antigen; HBsAg), which consists of three proteins encoded by a single *env* gene: large (L; pre-S1 + pre-S2 + S regions), middle (M; pre-S2 + S regions) and small (S; only S region). In particular, the pre-S1 (21–47, subtype *adr*) region of the L protein has been revealed to play a crucial role in human liver-specific HBV infection [1]. In 2003, we developed an HBsAg envelope L protein-derived nanoparticle, named bio-nanocapsule (BNC), as a human liver-specific carrier for a drug/gene delivery system [2]. BNC, which is composed of approximately 110 molecules of L protein and lipid bilayer, is overexpressed in recombinant

Abbreviations
BNC, bio-nanocapsule; GST, glutathione *S*-transferase; HBsAg, HBV surface antigen; HBV, hepatitis B virus; Lp, liposome; mAP, minimal albumin promoter; mFE, mouse fetoprotein enhancer; QCM, quartz crystal microbalance; SCCA1, squamous cell carcinoma antigen-1; SCID, severe combined immunodeficiency.

Saccharomyces cerevisiae as an approximately 50 nm hollow particle [3,4]. BNC is specifically accumulated in the human liver-derived cultured cells (*in vitro*) and even in the human liver-derived tumors in mice xenograft models (*in vivo*) [2,5]. Recently, BNC has been shown to spontaneously form a complex with adjunct liposomes (Lp) containing various large materials (e.g. 100 nm polystyrene beads and approximately 40 kbp plasmids), and the BNC-liposome (BNC-Lp) complex can also deliver these incorporated materials specifically to human liver-derived cells and tissues [6]. Because the pre-S1 region, especially pre-S1 (21–47), is crucial for the human liver-specific delivering ability of BNC and BNC-Lp, the attachment and cellular entry of BNC and BNC-Lp are postulated to be similarly mediated by the infection mechanism of HBV.

To develop BNC and BNC-Lp as drug/gene delivery system carriers targeted to the human liver for clinical use, it will be crucial to have animal models susceptible to HBV infection. However, the availability of higher primates (i.e. chimpanzees) is extremely limited, and their use is highly prohibited for both ethical and political reasons. Although the tree shrews *Tupaia belangeri* [7] and the urokinase-type plasminogen activator-transgenic severe combined immunodeficiency (SCID) mice transplanted with human hepatocytes [8] have recently been demonstrated to be useful for this purpose, the availability of these models is also quite poor. This dearth of appropriate models led us to establish a small animal model whose liver becomes sensitive to HBV infection by the liver-specific expression of HBV receptor.

Although numerous efforts have been made to identify an HBV receptor [9], no molecule has so far met two of the requirements: (a) the molecule directly binds to pre-S1 (21–47) and (b) its expression indeed enhances the cellular incorporation of HBV. In 2001, a squamous cell carcinoma antigen-1 (SCCA1) was shown to interact with tetrameric pre-S1 (21–47) peptides and facilitate the infection of HBV not only in human hepatic cells, but also in other cells by its ectopic expression [10,11], suggesting that SCCA1 is a promising candidate for HBV receptor. In the present study, with the aim of establishing a BNC-susceptible rodent model, we examined the effects of expression of SCCA1 on the cellular uptake of BNC both *in vitro* and *in vivo*. We provide evidence for the direct interaction of the recombinant SCCA1 protein with BNC, the competitive inhibition of the cell attachment of BNC to the human liver-derived cells by the SCCA1 protein, and the enhancement of the cellular uptake of BNC-Lp by the expression of SCCA1. In addition, we established a transgenic rat line that specifically expresses SCCA1 in the liver. When administered systemically, the amount of BNC in the liver was found to be increased by the expression of SCCA1. This animal model is expected to be useful for evaluating the therapeutic effect of BNC as a drug delivery system carrier, as well as for elucidating the extremely regulated infection mechanism of HBV.

Results

Hepatophilicity in the cell attachment of BNC

HBV specifically attaches to the human liver-derived cells before its cell entry [12]. We analyzed the attachment of BNC to various cell lines under microscopy. Cells were kept on ice for 2 min to repress the cellular uptake activity, and then attached with cytochrome 3 (Cy3)-BNC (i.e. Cy3-labeled BNC) on ice for 1 h (Fig. 1). After these treatments, strong fluorescence was observed in the human hepatocarcinoma cell lines HepG2 and Huh7 and weak fluorescence was observed in NuE cells. No fluorescence was detected in the other cell lines (i.e. rat hepatocarcinoma MH1C1 cells,

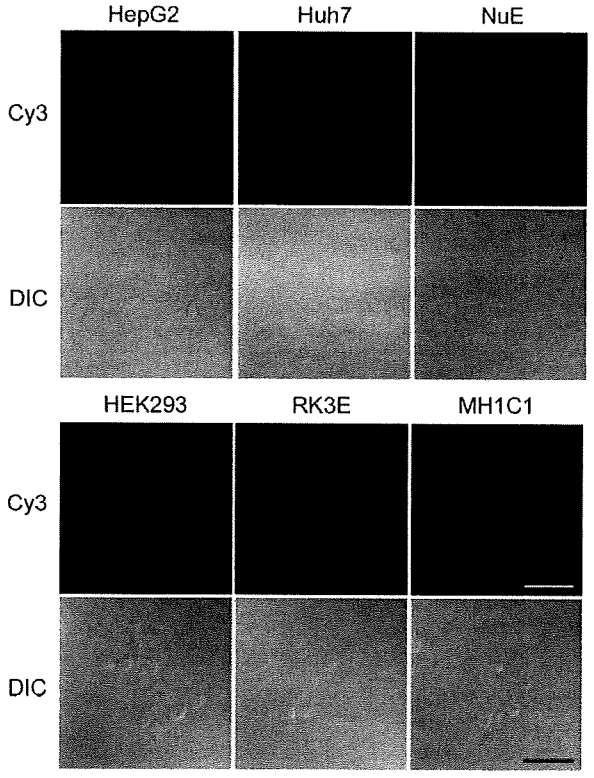

Fig. 1. Cell attachment of Cy3-BNC. HepG2, Huh7, NuE, HEK293, RK3E and MH1C1 cells were incubated with the Cy3-BNC for 1 h on ice and observed under a confocal laser microscope. Scale bar = 20 μm.

human embryonic kidney HEK293 cells and rat embryonic kidney RK3E cells) indicating that Cy3-BNC preferentially attaches onto the human liver-derived cells, as observed with HBV.

Interaction of SCCA1 with BNC

Recombinant SCCA1 protein was shown to interact directly with the pre-S1 (21–47) region and to inhibit the attachment of HBV to the human liver-derived cells [10,11]. To examine the behavior of SCCA1 to BNC, the recombinant glutathione *S*-transferase (GST)-SCCA1 protein was expressed in *Escherichia coli* cells and purified with affinity resins to > 95% purity as judged by SDS/PAGE analysis (Fig. 2A). Then, the direct interaction of SCCA1 with BNC was investigated using a quartz crystal microbalance (QCM). An Au electrode of the QCM equipment was successively treated with the solutions of the GST-SCCA1 protein (68 kDa) or GST (26 kDa), $NaCl/P_i$ for washing, skim milk for blocking the remaining Au surface, and finally BNC (6.4 MDa as a particle) [4]. Based on the amounts of GST-SCCA1 (13.4 ng) and GST (12.5 ng) adsorbed on the electrode, it was estimated that a mean ± SEM of 8.0 ± 1.4 μg (n = 4) of BNC were bound per nmol of GST-SCCA1, whereas only 0.2 μg of BNC was bound per nmol of GST alone (Fig. 2B). On the other hand, 514 ± 6.0 μg (n = 4) of BNC were bound per nmol of anti-preS2 mouse monoclonal IgG (180 kDa) adsorbed first on the electrode as a positive control. Thus, it was estimated that approximately 0.013 mol of BNC was bound per mol of GST-SCCA1 adsorbed on the Au surface, even though much less efficiently than the binding in the positive control (0.81 mol of BNC per mol of antibody).

Next, the Cy3-labeled BNC was preincubated with GST, GST-SCCA1 or heparin at 37 °C for 30 min, and then added to the culture medium of HepG2 cells. The fluorescent intensity was unchanged by preincuba-

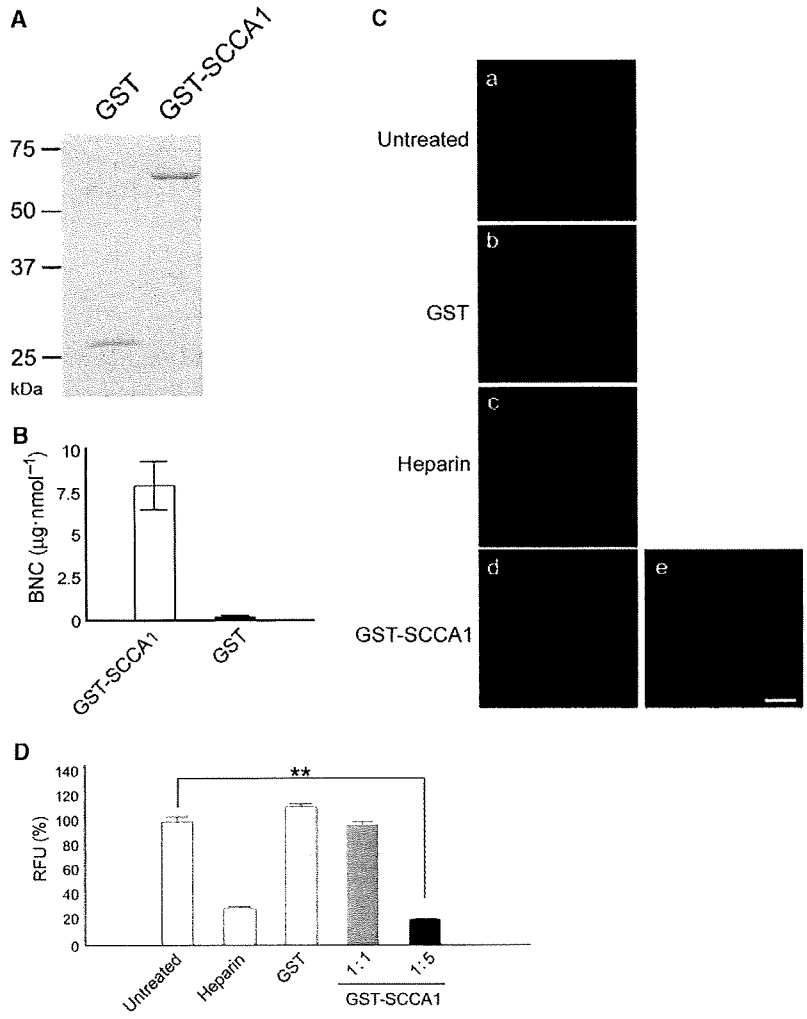

Fig. 2. Competition of cell attachment of BNC with the recombinant SCCA1 protein. (A) SDS/PAGE analysis of the purified recombinant GST-SCCA1. The molecular masses of GST and GST-SCCA1 are estimated to be 26 and 68 kDa, respectively. (B) Direct interaction between BNC and the recombinant GST-SCCA1 protein. The interaction was measured using QCM (n = 4, mean ± SEM). (C) Competition of the cell attachment of Cy3-BNC with the recombinant GST-SCCA1 protein. Cy3-BNC was incubated with HepG2 on ice for 1 h after preincubation with either a fivefold molar excess of GST (b), 100 $\mu g \cdot mL^{-1}$ heparin (c), an equimolar amount of GST-SCCA1 (d) or a fivefold molar excess of GST-SCCA1 (e) Scale bar = 20 μm. (D) Competition of the cell attachment of Cy3-BNC with the recombinant GST-SCCA1 protein. The relative fluorescence unit (RFU) was measured from the TIFF images taken under the same conditions as Fig. 2C (n = 4, mean ± SEM, $^{**}P < 0.01$, t-test).

tion with GST (Fig. 2C: b), whereas preincubation with heparin significantly decreased the attachment of the Cy3-BNC (Fig. 2C: c), as previously reported in studies using HBV [13]. Preincubation with an equimolar amount or with a 5-fold molar excess of GST-SCCA1 resulted in a decrease of fluorescence intensity in a dose-dependent manner (Fig. 2C: d,e and D). Taken together, these results indicate that SCCA1 is capable of interacting directly with BNC, as well as with HBV [10,11], and that the soluble SCCA1 protein inhibits the attachment of BNC to the surface of hepatic cells, presumably by competing with SCCA1 expressed on the cell surface.

Effect of SCCA1 on the transfection using the BNC-Lp complex

BNC was converted into the BNC-Lp complex by mixing with lipoplexes containing a luciferase expression plasmid. HepG2 cells were then incubated for 3 h with BNC-Lp, which was preincubated with heparin, GST or GST-SCCA1. After 3 days, the luciferase activity of each cell lysate was determined (Fig. 3A). As observed in the competition assay using Cy3-BNC (Figs 2C,D), heparin markedly inhibited the transfection using the BNC-Lp complex, whereas GST alone showed no effect. Preincubation with GST-SCCA1 decreased the transfection efficiency in a dose-dependent manner: the efficiency was 57 ± 14% at an equimolar amount of GST-SCCA1 and 35 ± 8.4% at a fivefold molar excess of GST-SCCA1. Next, three cell lines (HepG2, MH1C1 and HEK293) were transfected with pcDNA-SCCA1, and the stable expression of SCCA1 was confirmed by RT-PCR using a qualified set of SCCA1-specific primers [14] and western blotting (Fig. 3B). Faint bands observed in two human-derived cell lines, HepG2 and HEK293, without transfection were likely amplified from the endogenous *SCCA1* mRNA. These cell lines, along with the parental

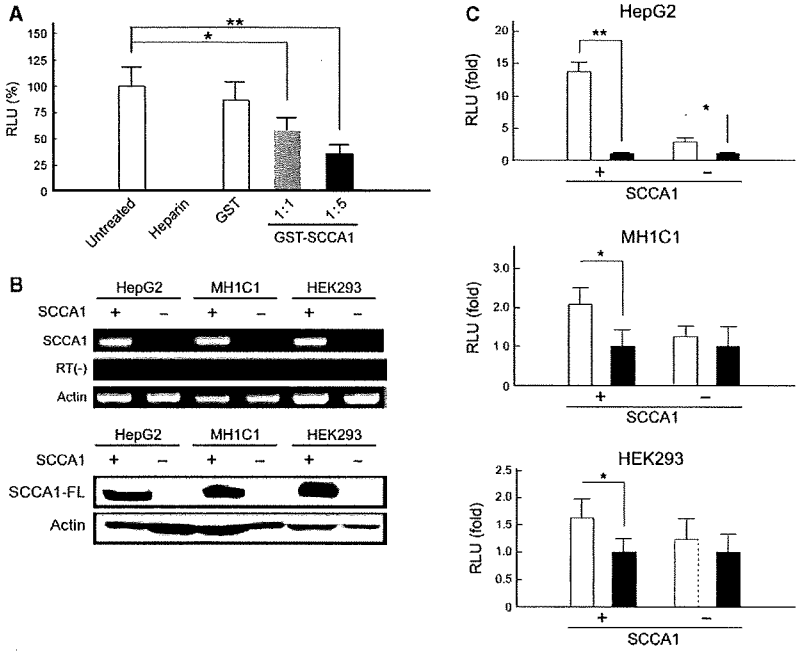

Fig. 3. Effect of SCCA1 on cellular uptake of the BNC-Lp complex. (A) Transfection efficiency of the BNC-Lp complex in HepG2 cells. The BNC-Lp complex containing the luciferase expression vector was added to the medium of HepG2 cells after preincubation with either a fivefold molar excess of GST, 100 μg·mL^{-1} heparin, an equimolar amount of GST-SCCA1 (gray bar) or a fivefold molar excess of GST-SCCA1 (black bar). Cells were incubated with BNC-Lp for 3 h and cultured for 72 h in fresh medium. The transfection efficiency was determined using relative luminescence units (RLU), which were normalized to protein concentrations (n = 4, mean ± SD, *P < 0.05, **P < 0.01, t-test). (B) Establishment of the SCCA1-expressing HepG2, MH1C1 and HEK293 cells. RT-PCR was performed using 1 μg of total RNA as a template (upper panels). RT(–) shows the results of conventional PCR using total RNA as a template. Ten microgram (as protein) of cell lysate was subjected to western blotting using anti-FLAG serum (lower panels). The mRNA and protein of actin were used as an internal control. (C) Transfection efficiency of the BNC-Lp complex in the SCCA1-expressing cell lines. Cells were incubated with BNC-Lp (white bars) or Lp (black bars) for 3 h and cultured for 72 h in fresh medium. The RLU of each cell line transfected with BNC-Lp was normalized by that of the cells transfected with Lp only (n = 4, mean ± SD, *P < 0.05, **P < 0.01, t-test).

cells, were further transfected with the BNC-Lp complex or Lp only containing the luciferase gene. As shown in Fig. 3C, the luciferase activities of the SCCA1-expressing cell lines transfected with BNC-Lp complex were considerably higher than those with Lp only (1.6–13.7-fold increases). The parental HepG2 cells transfected with BNC-Lp showed higher luciferase activity than those with Lp only, as described previously [6], whereas parental MH1C1 and HEK293 cells did not show significant differences between BNC-Lp complex and Lp. These results suggest that the expression of SCCA1 contributed not only to the attachment of BNC, but also to the cellular uptake.

Establishment of transgenic rats expressing SCCA1

The SCCA1-FLAG cDNA was placed in the region downstream of the mouse fetoprotein enhancer (mFE) and the mouse minimal albumin promoter (mAP) and upstream of the polyadenylation region of a rodent liver-specific transgene expression vector pLIVE™ (Mirus Bio Corp., Madison, WI, USA). The whole construct was inserted between the mouse H19 insulators of pWHERE vector (InvivoGen, San Diego, CA, USA). The expression cassette was linearized with *Pac*I and then injected into the pronucleus of fertilized eggs obtained from Wistar rats. Finally, five lines were confirmed to harbor the SCCA1-transgene in their germ lines by a genomic PCR assay using rat tails. Using an immunoprecipitation assay, all founders were shown to express the SCCA1-FLAG protein to a similar extent in their livers (data not shown). Among the tissues derived from line 3, the *SCCA1-FLAG* mRNA was detected exclusively in the liver (Fig. 4A, upper panel) and the SCCA1-FLAG protein was also detected in the liver (Fig. 4A, lower panel). Based on the sensitivity of western blotting using anti-FLAG serum (approximately 2 ng per lane), the SCCA1-FLAG protein was not detected by western blotting even when approximately 10 μg (as protein per lane) of the liver homogenate was used (data not shown), which indicates the content of SCCA1-FLAG in liver is less than 0.02% (w/w) of total soluble protein.

Transfection of rat primary hepatocytes using the BNC-Lp complex

Primary hepatocytes were isolated from the transgenic rat liver and subjected to the transfection using the BNC-Lp complex (Fig. 4B). Compared with the hepatocytes from the wild-type rats, the SCCA1-transgenic rat-derived hepatocytes transfected with BNC-Lp expressed an approximately 3.7-fold higher

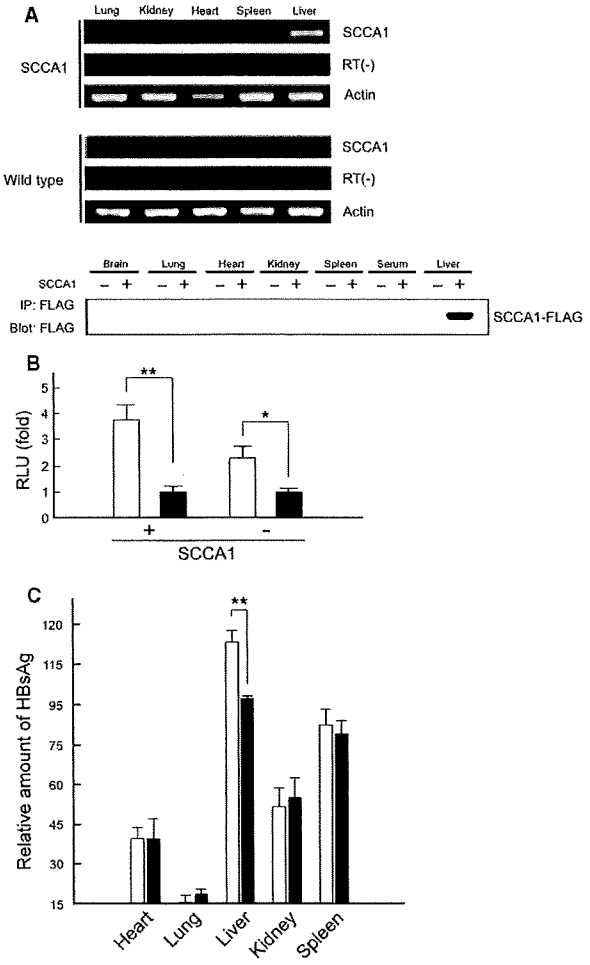

Fig. 4. Analyses of the transgenic rats expressing SCCA1. (A) Liver-specific expression of SCCA1. RT-PCR was performed using 1 μg of total RNA as a template (upper panels show SCCA1-transgenic rats; middle panels show wild-type rats). RT(–) shows the results of conventional PCR using total RNA as a template. Ten miligrams (as protein) of tissue homogenate was subjected to the immunoprecipitation assay using anti-FLAG serum (lower panel). The mRNA and protein of actin were used as an internal control. (B) Transfection efficiency of the BNC-Lp complex in the rat primary hepatocytes expressing SCCA1. The hepatocytes were incubated with BNC-Lp (white bars) or Lp (black bars) for 3 h and cultured for 72 h in fresh medium. RLU of the primary hepatocytes transfected with BNC-Lp was normalized by that of the hepatocytes transfected with Lp ($n = 4$, mean ± SD, $^*P < 0.05$, $^{**}P < 0.01$, *t*-test). (C) Tissue homogenates of either the transgenic (white bars) or wild-type rats (black bars), which received intravenous injection of BNC 1.5 h before sacrifice, were subjected to an IMx assay system to quantify the relative amount of BNC (three rats for each measurement and three measurements for each value, mean ± SD, $^{**}P < 0.01$, *t*-test).

luciferase activity than those transfected with Lp only, whereas the wild-type rat-derived hepatocytes transfected with BNC-Lp showed 2.3-fold higher activitity than those with Lp only. These results indicate that the expression of SCCA1 promoted either the attachment of BNC or the cellular uptake, as observed for the stable cell lines (Fig. 3C). Because the HBV *env*-derived materials (the HBsAg S particle [15] and a pre-S1 (2–48) synthetic lipopeptide [16]) are accumulated in the mouse liver specifically, BNC-Lp may be preferentially incorporated by wild-type rat-derived primary hepatocytes.

Biodistribution of BNC in SCCA1-transgenic rats

The SCCA1-transgenic rats were administered with BNC systemically using the tail vein and sacrificed after 1.5 h. Homogenates of various tissues were subjected to an ELISA for BNC to measure the relative amounts of BNC incorporated into (or associated with) these tissues (Fig. 4C). BNC was detected in the heart, lung, liver, kidney and spleen, but not in the serum. In particular, BNC was significantly accumulated in the livers and spleens of both the transgenic and wild-type rats. However, only liver tissue showed a significant difference in the amount of BNC between the transgenic and wild-type rats. The transgenic rat livers accumulated an approximately 1.2-fold greater amount of BNC compared to their wild-type counterparts, suggesting that the expression of SCCA1 enhanced the accumulation of BNC in the liver.

Uptake of BNC by the SCCA1-expressing rat hepatocytes

Cryosections were prepared from the livers of rats that had received intravenous injection of Cy3-BNC 1.5 h before sacrifice, immunostained with markers of hepatocytes, endothelial cells, and macrophages (including Küppfer cells) (albumin, CD44 and Mac-1, respectively) and visualized with fluorescein (Figs 5 and 6). When the sections were examined for albumin, the fluorescence derived from Cy3 and fluorescein was found to be well-merged in certain regions of the transgenic rat liver, indicating that the Cy3-BNC had been accumulated partly in the hepatocytes expressing SCCA1 (Fig. 5A, upper panels). A high magnification image also suggested that Cy3-BNC had been incorporated into the hepatocytes with extensive albumin production (Fig. 5B). The remaining Cy3-BNC may have been entrapped in the hepatic sinusoidal structure. By contrast, in the wild-type rat liver, the fluorescence derived from both dyes was not merged in any field (Fig. 5A, lower panels). Similarly, immunostaining with CD44 and Mac-1 did not show any merged portion in the livers of either transgenic or wild-type rats, indicating that Cy3-BNC was localized in neither endothelial cells, nor macrophages (Fig. 6A,B). Collectively, these findings suggest that SCCA1 expression

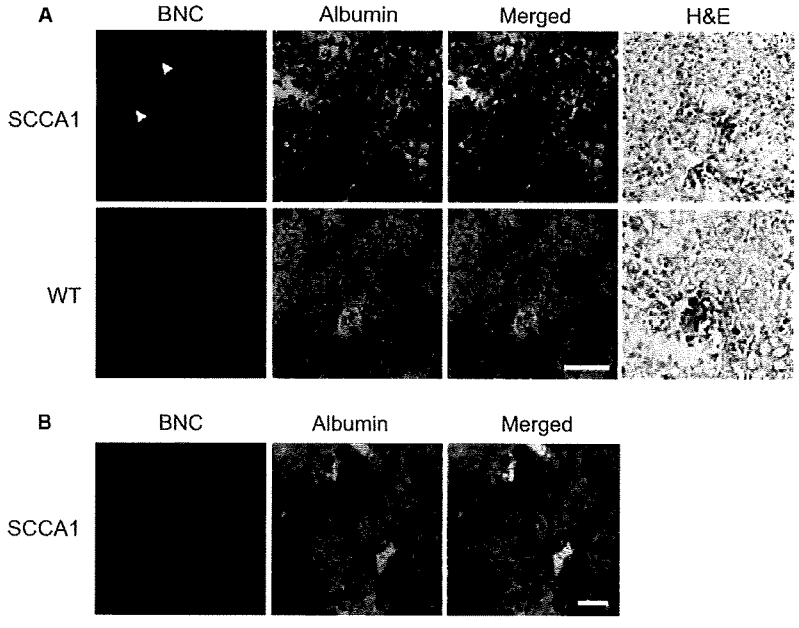

Fig. 5. Immunohistological analysis using anti-albumin serum of rat liver after the intravenous injection of Cy3-BNC. (A) Liver cryosections of the rats receiving the Cy3-BNC injection were immunostained with an anti-albumin serum. Arrowheads indicate the colocalized positions of the Cy3-BNC and albumin. Scale bar = 50 μm. (B) Zoom-up of the colocalized positions. Scale bar = 20 μm. H&E, hematoxylin and eosin; WT, wild-type.

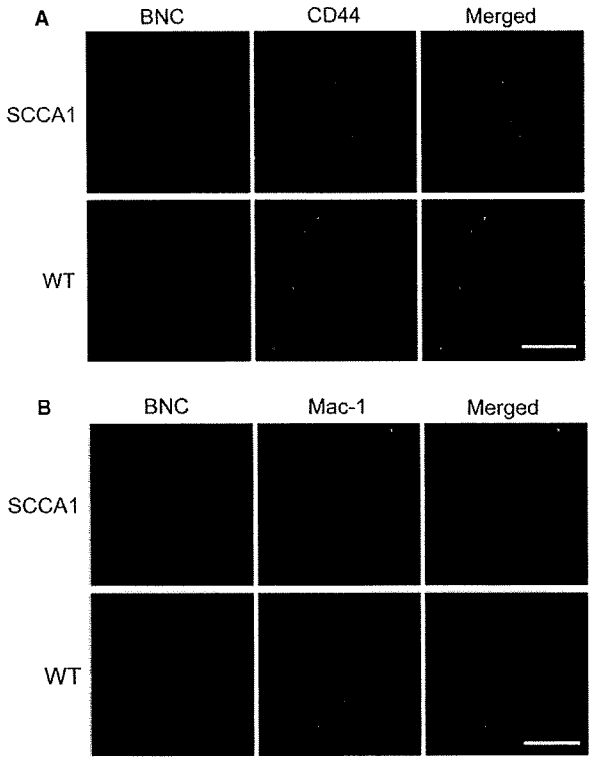

Fig. 6. Immunohistological analysis using either anti-CD44 and anti-Mac-1 sera of rat liver after the intravenous injection of Cy3-BNC. (A) Liver cryosections of the rats receiving the Cy3-BNC injection were immunostained with anti-CD44 serum. Scale bar = 50 μm. (B) Liver cryosections of the rats receiving the Cy3-BNC injection were immunostained with anti-Mac-1 serum. Scale bar = 50 μm. WT, wild-type.

might enable the incorporation of BNC into hepatocytes in the rat liver.

Discussion

SCCA1 is genetically classified as an ovalbumin-like serpin [17] and is commonly expressed in endothelial cells in humans. SCCA1 has been shown to function as an inhibitor of lysosomal cysteine proteases such as cathepsin K/L/S [18,19]. Furthermore, SCCA1 has recently been indicated to inhibit the phosphorylation activity of c-Jun N-terminal kinase by direct interaction [20]. It has also been demonstrated that cell surface expression of SCCAs, including SCCA1, is increased in HepG2 cells by stimulation with a pre-S1 (21–47) synthetic peptide [21] and that hepatocellular carcinoma cells proliferating in patients express abundant amounts of SCCA1 and other SCCAs [22]. These findings strongly suggest that SCCA1 is a pluripotent protein. Concerning the role of SCCA1 in HBV infection, two groups have reported that expression of SCCA1 enhances HBV infection in various cells *in vitro*. One of these groups first isolated SCCA1 as a ligand of the tetrameric pre-S1 (21–47) peptide and showed that expression of SCCA1 enhances HBV infection and that recombinant SCCA1 inhibits HBV infection [10]. Another group demonstrated that the SCCA1-mediated HBV infection does not involve the hepatic serpin clearance system [11]. The *in vitro* experiments described in the present study (Fig. 2) also confirmed that the attachment of BNC to the human liver-derived cells is inhibited by the recombinant SCCA1 protein, such as HBV, and that the incorporation of the BNC-Lp complex is enhanced by SCCA1 expression (Fig. 3). Additionally, we show for the first time the direct interaction of SCCA1 protein with BNC by QCM. Moreover, by the combined use of the enhancer/promoter cassette including mFE and mAP and the H19 insulators, we succeeded in generating transgenic rat strains that efficiently expressed SCCA1 in their liver and examined whether the hepatocytes became receptive to BNC, instead of HBV.

After the intravenous injection into the wild-type and SCCA1-expressing transgenic rats, BNC were immediately distributed to various tissues. Nevertheless, a significant portion of the injected BNC was found to be accumulated in the livers of both transgenic and wild-type rats. By comparing the ELISA data that demonstrate considerable accumulation of BNC in the liver (Fig. 4C) with the fluorescence intensity observed in limited areas (Fig. 5A), most BNC in the liver may have been entrapped in the hepatic sinusoidal structures. Analysis of the distribution of BNC within the transgenic rat liver indicated that at least 20% of BNC was localized specifically in the SCCA1-expressing hepatocytes, which was corroborated by the enhanced uptake of the BNC-Lp complex by the SCCA1-expressing rat hepatocytes (Fig. 4B). The remaining 80% of BNC was considered to be accumulated in the transgenic rat liver in both a nonspecific and a specific manner, namely, a large number of nano-scaled compounds have been shown to be entrapped by the liver nonspecifically [23], whereas the HBV *env*-derived materials (the HBsAg S particle [15] and a pre-S1 (2–48) synthetic lipopeptide [16]) are accumulated in the mouse liver specifically.

HBV is a causative factor for a highly infectious disease. The transient expression of SCCA1 in the liver of NOD/SCID mice has been reported to extend the retention of HBV in those livers [24], suggesting that long-term expression of SCCA1 could

achieve the establishment of HBV-susceptible mouse model. Although our transgenic rat model showed potential as an animal model of HBV infection, it is uncertain whether the efficiency of the SCCA1-expressing rat hepatocytes at incorporating HBV is sufficient for this purpose. Many cellular molecules have so far been proposed as HBV receptors (e.g. annexin V [25] and ASGPR [26]), but none of these molecules fulfills both of the requirements described above [i.e. direct interaction with pre-S (21–47) and enhancement of HBV infection by its expression]. Simultaneous expression of these molecules with SCCA1 might be expected to synergistically enhance the hepatocellular uptake of HBV, as well as BNC, in the transgenic rat model.

Experimental procedures

BNC and fluorescence-labeled BNC

The BNC was purified from *S. cerevisiae* AH22R$^-$ cells transformed with the HBsAg L protein-expression plasmid pGLDLIIP39-RcT, as previously described [4]. For visualization, the BNC was labeled with a FluoroLink™ Cy3 bisfunctional reactive dye (GE Healthcare, Chalfont St Giles, UK) according to the manufacturer's protocol. The Cy3-BNC was purified through a Superdex S-50 gel filtration column (GE Healthcare). The average size and Z-potential of the BNC were measured in NaCl/P_i (pH 7.4) at 25 °C by dynamic light scattering using a Zetasizer Nano-ZS (Malvern Instruments Ltd, Malvern, UK): 42.13 ± 1.68 nm (n = 3, mean ± SD, polydispersity index < 0.250) and −6.25 ± 4.22 mV (n = 3, mean ± SD) for BNC; 43.00 ± 2.16 nm (n = 3, mean ± SD, polydispersity index < 0.250) and −10.4 ± 7.76 mV (n = 3, mean ± SD) for Cy3-BNC, respectively.

Plasmids

Total RNA was extracted from HepG2 cells and purified using a TRI reagent (Invitrogen, Carlsbad, CA, USA). Reverse transcription was performed with a SuperScript III One-Step RT-PCR System and Platinum Taq High Fidelity using the primers: N-primer, 5′-GTTCACCATGAATTCA CTCAGTGAAGCC-3′, and C-primer, 5′-GCAATCAGT TTACCAGAACATCTGCAG-3′. The amplified SCCA1 sequence is the same as that reported in De Falco *et al.* [10], and harbors three amino acid substitutions in comparison with the original SCCA1 [27]. For bacterial expression of N-terminally GST-fused SCCA1 (GST-SCCA1), the amplified SCCA1 cDNA fragment (1.2 kbp) was subcloned into pGEX-6P-1 (GE Healthcare) to obtain pGEX-SCCA1. For mammalian expression as a C-terminally FLAG epitope-tagged protein (SCCA1-FLAG), the fragment was subcloned into the pcDNA3.1 vector (Invitrogen) to obtain pcDNA-SCCA1.

Cell cultures

HepG2 and Huh7 (human hepatocellular carcinoma), RK3E (rat embryonic kidney), MH1C1 (rat hepatocellular carcinoma) and HEK293 (human embryonic kidney) cells were cultured in DMEM (Nakalai Tesque, Kyoto, Japan) supplemented with 10% (v/v) fetal bovine serum and antibiotics (penicillin–streptomycin; Invitrogen). Cells were propagated at 37 °C in a humidified atmosphere of 5% CO_2. RPMI-1640 medium (Nakalai Tesque) was used for the culture of NuE (human hepatocellular carcinoma) cells. To obtain the cell lines stably expressing SCCA1, pcDNA-SCCA1 was transfected into HepG2, HEK293 and MH1C1 using a Calcium Phosphate Transfection kit (Invitrogen), and these transfectants were cultured in the appropriate medium containing G418 (Nakalai Tesuque). Rat hepatocytes were isolated from liver by perfusion with collagenase (Sigma, St Louis, MO, USA) according to the method of Seglen [28]. Approximately 1×10^6 cells were seeded onto a six-well collagen I coated-polystyrene plate (Iwaki, Tokyo, Japan) and cultured in William's Medium E (Invitrogen) supplemented with 15% fetal bovine serum, 1 nM insulin (Sigma) and 1 nM dexamethazone (Sigma). After 6 h, the medium was changed to William's Medium E (Invitrogen) supplemented with 15% fetal bovine serum.

Binding assay

Approximately 1×10^4 cells cultured for 36 h in an eight-well glass bottom chamber (Nalge Nunc, Naperville, IL, USA) were washed with ice-cold NaCl/P_i three times, and incubated with Cy3-BNC (1 μg as HBsAg L protein in 200 μL of culture medium) on ice for 1 h. The cells were fixed in 4% (w/v) paraformaldehyde in NaCl/P_i, and observed under an FV-1000D confocal laser microscope (Olympus, Tokyo, Japan). The relative fluorescence unit was measured from the TIFF files taken under the same conditions. Five cells in the same visualizing field were analyzed utilizing software MetaMorph (Universal Imaging, Sunnyvale, CA, USA).

Expression and purification of GST-SCCA1

Cells of the *E. coli* strain BL21 (Stratagene, La Jolla, CA, USA) transformed with pGEX-SCCA1 were cultured in LB broth containing 1 mM isopropyl thio-β-D-galactoside for 3 h at 30 °C. The GST-SCCA1 was purified from the cell lysate with Glutathione Sepharose 4B resins (GE Healthcare) according to the manufacturer's protocol, and stored at −80 °C. The purity was determined by SDS/PAGE) followed by staining with Coomassie brilliant blue R250.

QCM

The amount of BNC bound to the recombinant SCCA1 was measured at 25 °C using a QCM model Twin-Q (As One, Osaka, Japan), which has two 500 μL cells equipped with 27 MHz QCM plates. The Au electrode in the cell was coated with either GST, GST-SCCA1 (~ 15 ng) or monoclonal anti-preS2 region serum (positive control; Institute of Immunology, Co. Ltd, Tokyo, Japan), washed with $NaCl/P_i$, and blocked with 150 $\mu g \cdot mL^{-1}$ skim milk in $NaCl/P_i$. The adsorption of BNC onto GST, GST-SCCA1 or the antibody was monitored by the frequency change, of which 1 Hz corresponds to 30 pg of the adsorbed protein.

Transfection assay using the BNC-Lp complex

BNC spontaneously forms a complex with Lp containing various materials (e.g. DNA, chemicals, and polystyrene beads), enabling the delivery of these materials specifically to the target cells *ex vivo* and *in vivo* according to the tropism of BNC [6]. A freeze-dried form of cationic liposomes (1.5 mg as lipids; Coatsome EL-01-D; NOF Corp., Tokyo, Japan) was mixed with a firefly-derived luciferase-expression vector pGL3-Luc (250 μg; Promega, Madison, WI, USA) to form a lipoplex (the liposome-DNA complex). The lipoplex comprising 100 μg of liposome and 16.7 μg of DNA was incubated with BNC (100 μg as HBsAg L protein) for 15 min at room temperature to allow formation of the BNC-Lp complex. Approximately 4×10^5 cells in a 24-well plate or approximately 4×10^6 cells in a six-well plate were incubated with the BNC-Lp complex at a concentration of 2 μg (as HBsAg L protein)$\cdot mL^{-1}$ for 3 h, and then cultured in fresh medium for 72 h. The luciferase activity of each cell lysate was measured using a Luciferase Assay System (Promega).

Competition assay

Either the Cy3-BNC or the BNC-Lp complex harboring pGL3-Luc was incubated with a fivefold molar excess of GST or an equimolar amount or a fivefold molar excess of GST-SCCA1 for 30 min at 37 °C. As a positive control, the BNC and BNC-Lp were incubated in 100 $\mu g \cdot mL^{-1}$ of heparin. Aliquots containing BNC or BNC-Lp were subjected to binding and transfection assays.

RT-PCR and western blotting

Total RNAs of the cultured cells and rat tissues were extracted using a TRI reagent (Invitrogen) and subjected to RT-PCR with a Superscript one-step RT-PCR with platinum Taq (Invitrogen) using 1 μg of total RNA as a template. The set of primers comprised: sense primer, 5′-TCCAGAAGCTTGAAGAGAAAC-3′; anti-sense primer, 5′-TGTAGGACTCCAGATAGCACG-3′. Both sequences were already confirmed to amplify the SCCA1 mRNA specifically [14]. Control experiments without reverse-transcription [RT(−)] were performed utilizing conventional PCR mixture with recombinant Taq polymerase (Takara, Kyoto, Japan) using 1 μg of total RNA as a template to exclude the possibility of contamination of genomic DNA. The amplified DNA fragments were analyzed by electrophoresis using 2% (w/v) agarose. For western blotting, 10 μg (as protein) of total cell lysate was subjected to 12.5% SDS/PAGE, electrically transferred to a poly(vinylidene difluoride) membrane (Immobilon-P; Millipore, Billerica, MA, USA), and immunoblotted with monoclonal anti-FLAG M2 (Sigma; 1 : 1000) or anti-actin (Sigma; 1 : 1000) sera followed by horseradish peroxidase-conjugated goat anti-(mouse IgG) serum (GE Healthcare; 1 : 5000). The blots were visualized by enhanced chemiluminescence (ECL plus; GE Healthcare) using a luminescence detector Chemi-Doc (Bio-Rad, Hercules, CA, USA).

SCCA1 transgenic rats

All animal experiments were approved by the Committee for Experimental Animal Science of the Institute for Scientific and Industrial Research, Osaka University. Animals were treated according to the guidelines for the use of experimental animals provided by the Ministry of Education, Culture, Sports, Science and Technology, Japan. To establish transgenic rats overexpressing SCCA1 specifically in the hepatocytes, the DNA fragment encoding SCCA1-FLAG cDNA was inserted between *Nhe*I and *Sma*I sites of the pLIVE™ vector (Mirus Bio Corp., Madison, WI, USA) to place under a mFE and a mouse mAP. The *Bgl*II-*Nde*I expression cassette encoding mFE, SCCA1-FLAG, and the polyadenylation region was blunted and then inserted between *Sma*I and *Hpa*I sites of the pWHERE vector (InvivoGen) to place between the mouse H19 insulators. The plasmid was digested with *Pac*I, and an approximately 7.4 kbp fragment containing the SCCA1 expression cassette encompassing both insulators was injected into the pronucleus of fertilized eggs (Wistar rats), and the injected embryos were transferred into pseudopregnant recipients. Transgenic rats were identified by PCR using genomic DNA extracted from tail biopsies.

Immunoprecipitation assay

Rat tissues were isolated immediately after sacrifice, frozen in liquefied nitrogen, and stored at −80 °C. Tissues were homogenized with a homogenizer (Multipro 395; Dremel Corp., Racine, WI, USA) in a threefold volume of lysis buffer [50 mM Tris–HCl (pH 8.0), 150 mM NaCl, 0.5% (v/v) Triton-X 100, 1 mM EDTA, and 0.005% (w/v) sodium azide]. The supernatants of homogenates (5 mg of protein) were mixed with anti-FLAG M2 serum (2 μg), incubated at 4 °C for 1 h, mixed with protein G-Sepharose

4B beads [40 μL (50% slurry); GE Healthcare], washed three times with lysis buffer, and then boiled in Laemmli's sample buffer. Western blotting was performed as described above.

Biodistribution analysis

Transgenic rats received an intravenous injection of BNC (0.5 $mg \cdot kg^{-1}$ body weight) and were sacrificed 1.5 h after the injection. Rat tissue homogenates (see above) were diluted with a 10-fold volume of lysis buffer and subjected to the ELISA for BNC using an IMx HBsAg assay system (Abbott Japan, Tokyo, Japan).

Immunohistochemistry

Transgenic rats received an intravenous injection of the Cy3-BNC (1.0 $mg \cdot kg^{-1}$ body weight) and were sacrificed 1.5 h after the injection. The rat livers were rapidly frozen and cryosectioned at 5 μm, fixed in 10% paraformaldehyde in $NaCl/P_i$ for 5 min, permeabilized in blocking buffer [$NaCl/P_i$ containing 10% (v/v) normal sheep serum] at room temperature for 1 h, and then incubated at 4 °C overnight in the blocking buffer containing one of the following 100-fold diluted primary mouse monoclonal antibodies; anti-albumin (Bethyl Laboratories, Montgomery, TX, USA), anti-CD44 (BD Bioscience, San Jose, CA, USA) and anti-Mac-1(Chemicon International, Temecula, CA, USA). The sections were washed twice with $NaCl/P_i$, and then incubated with a 2% (v/v) fluorescein isothiocyanate-conjugated goat anti-(mouse IgG) serum (Rockland, Gilbertsville, PA, USA) in $NaCl/P_i$ at room temperature for 1 h. The fluorescence was observed under a confocal laser scanning microscope. Several sections were subjected to the counterstaining with hematoxylin and eosin.

Acknowledgements

The authors thank Professors M. Seno (Okayama University) and P. Pontisso (Padova University) for supplying the *SCCA1* gene; T. Tadakuma (National Defense Medical College) for providing the NuE cells; and K. Isoda and M. Kondo (Osaka University) for their advice on the primary culture of hepatocytes. We are also grateful to Professors A. Kondo (Kobe University) and M. Ueda (Keio University) for their helpful advice and to Ms Y. Matsushita (Osaka University) for her technical support. This work was supported by a Grant-in-Aid for Scientific Research on Priority Areas (#18015032) from the Ministry of Education, Culture, Sports, Science and Technology of Japan, a Grant-in-Aid for Research on Advanced Medical Technology from the Ministry of Health, Labour and Welfare of Japan, a research grant for the 'Creation of bio-devices and bio-systems with chemical and biological molecules for medical use (CREST)', and a research grant from the Regional Research and Development Resources Utilization Program of the Japan Science and Technology Agency (JST).

References

1 Neurath AR, Kent SB, Strick N & Parker K (1986) Identification and chemical synthesis of a host cell receptor binding site on hepatitis B virus. *Cell* **46**, 429–436.
2 Yamada T, Iwasaki Y, Tada H, Iwabuki H, Chuah MK, VandenDriessche T, Fukuda H, Kondo A, Ueda M, Seno M *et al.* (2003) Nanoparticles for the delivery of genes and drugs to human hepatocytes. *Nat Biotechnol* **21**, 885–890.
3 Kuroda S, Otaka S, Miyazaki T, Nakao M & Fujisawa Y (1992) Hepatitis B virus envelope L protein particles: synthesis and assembly in *Saccharomyces cerevisiae*, purification and characterization. *J Biol Chem* **267**, 1953–1961.
4 Yamada T, Iwabuki H, Kanno T, Tanaka H, Kawai T, Fukuda H, Kondo A, Seno M, Tanizawa K & Kuroda S (2001) Physicochemical and immunological characterization of hepatitis B virus envelope particles exclusively consisting of the entire L (pre-S1 pre-S2 S) protein. *Vaccine* **19**, 3143–3163.
5 Iwasaki Y, Ueda M, Yamada T, Kondo A, Seno M, Tanizawa K, Kuroda S, Sakamoto M & Kitajima M (2007) Gene therapy of liver tumors with human liver-specific nanoparticles. *Cancer Gene Ther* **14**, 74–81.
6 Jung J, Matsuzaki T, Tatematsu K, Okajima T, Tanizawa K & Kuroda S (2008) Bio-nanocapsule conjugated with liposomes for in vivo pinpoint delivery of various materials. *J Control Release* **126**, 255–264.
7 Köck J, Nassal M, MacNelly S, Baumert TF, Blum HE & von Weizsäcker F (2001) Efficient infection of primary tupaia hepatocytes with purified human and woolly monkey hepatitis B virus. *J Virol* **75**, 5084–5089.
8 Tateno C, Yoshizane Y, Saito N, Kataoka M, Utoh R, Yamasaki C, Tachibana A, Soeno Y, Asahina K, Hino H *et al.* (2004) Near completely humanized liver in mice shows human-type metabolic responses to drugs. *Am J Pathol* **165**, 901–912.
9 Glebe D & Urban S (2007) Viral and cellular determinants involved in hepadnaviral entry. *World J Gastroenterol* **13**, 22–38.
10 De Falco S, Ruvoletto MG, Verdoliva A, Ruvo M, Raucci A, Marino M, Senatore S, Cassani G, Alberti A, Pontisso P *et al.* (2001) Cloning and expression of a novel hepatitis B virus-binding protein from HepG2 cells. *J Biol Chem* **276**, 36613–36623.

11 Moore PL, Ong S & Harrison TJ (2003) Squamous cell carcinoma antigen 1-mediated binding of hepatitis B virus to hepatocytes does not involve the hepatic serpin clearance system. *J Biol Chem* **278**, 46709–46717.
12 Qiao M, Macnaughton TB & Gowans EJ (1994) Adsorption and penetration of hepatitis B virus in a nonpermissive cell line. *Virology* **201**, 356–363.
13 Chulze A, Gripon P & Urban S (2007) Hepatitis B virus infection initiates with a large surface protein-dependent binding to heparan sulfate proteoglycans. *Hepatology* **46**, 1759–1768.
14 Murakami A, Suminami Y, Sakaguchi Y, Nawata S, Numa F, Kishi F & Kato H (2000) Specific detection and quantitation of SCC antigen 1 and SCC antigen 2 mRNAs by fluorescence-based asymmetric semi-nested reverse transcription PCR. *Tumor Biol* **21**, 224–234.
15 Ohta A, Sekimoto M, Sato M, Koda T, Nishimura S, Iwakura Y, Sekikawa K & Nishimura T (2000) Indispensable role for TNF-alpha and IFN-gamma at the effector phase of liver injury mediated by Th1 cells specific to hepatitis B virus surface antigen. *J Immunol* **165**, 956–961.
16 Petersen J, Dandri M, Mier W, Lütgehetmann M, Volz T, von Weizsäcker F, Haberkorn U, Fischer L, Pollok JM, Erbes B *et al.* (2008) Prevention of hepatitis B virus infection in vivo by entry inhibitors derived from the large envelope protein. *Nat Biotechnol* **26**, 335–341.
17 Silverman GA, Whisstock JC, Askew DJ, Pak SC, Luke CJ, Cataltepe S, Irving JA & Bird PI (2004) Human clade B serpins (ov-serpins) belong to a cohort of evolutionarily dispersed intracellular proteinase inhibitor clades that protect cells from promiscuous proteolysis. *Cell Mol Life Sci* **61**, 301–325.
18 Schick C, Pemberton PA, Shi GP, Kamachi Y, Cataltepe S, Bartuski AJ, Gornstein ER, Brömme D, Chapman HA & Silverman GA (1998) Cross-class inhibition of the cysteine proteinases cathepsins K, L, and S by the serpin squamous cell carcinoma antigen 1: a kinetic analysis. *Biochemistry* **37**, 5258–5266.
19 Masumoto K, Sakata Y, Arima K, Nakao I & Izuhara K (2003) Inhibitory mechanism of a cross-class Serpin, the squamous cell carcinoma antigen 1. *J Biol Chem* **278**, 45296–45304.
20 Katagiri C, Nakanishi J, Kadoya K & Hibino T (2006) Serpin squamous cell carcinoma antigen inhibits UV-induced apoptosis via suppression of c-JUN NH2-terminal kinase. *J Cell Biol* **172**, 983–990.
21 Ruvoletto MG, Tono N, Carollo D, Vilei T, Trentin L, Muraca M, Marino M, Gatta A, Fassina G & Pontisso P (2004) Surface expression of squamous cell carcinoma antigen (SCCA) can be increased by the preS1 (21–47) sequence of hepatitis B virus. *J Gen Virol* **85**, 621–624.
22 Pontisso P, Calabrese F, Benvegnù L, Lise M, Belluco C, Ruvoletto MG, Marino M, Valente M, Nitti D, Gatta A *et al.* (2004) Overexpression of squamous cell carcinoma antigen variants in hepatocellular carcinoma. *Br J Cancer* **90**, 833–837.
23 Owens DE III & Peppas NA (2006) Opsonization, biodistribution, and pharmacokinetics of polymeric nanoparticles. *Int J Pharm* **307**, 93–102.
24 Xia HB, Chen ZY & Chen XG (2006) Overexpression of hepatitis B virus-binding protein, squamous cell carcinoma antigen 1, extends retention of hepatitis B virus in mouse liver. *Acta Biochim Biophys Sin (Shanghai)* **38**, 484–491.
25 De Meyer S, Depla E, Maertens G, Soumillion A & Yap SH (1999) Characterization of small hepatitis B surface antigen epitopes involved in binding to human annexin V. *J Viral Hepatol* **6**, 277–285.
26 Hertogs K, Leenders WP, Depla E, De Bruin WC, Meheus L, Raymackers J, Moshage H & Yap SH (1993) The asialoglycoprotein receptor mediates hepatic binding and uptake of natural hepatitis B virus particles derived from viraemic carriers. *Virology* **197**, 549–557.
27 Suminami Y, Kishi F, Sekiguchi K & Kato H (1991) Squamous cell carcinoma antigen is a new member of the serine protease inhibitors. *Biochem Biophys Res Commun* **181**, 51–58.
28 Seglen PO (1976) Preparation of isolated rat liver cells. *Methods Cell Biol* **13**, 29–83.

The fusing ability of sperm is bestowed by CD9-containing vesicles released from eggs in mice

Kenji Miyado*†‡§, Keiichi Yoshida‡¶, Kazuo Yamagata‖, Keiichi Sakakibara*, Masaru Okabe**, Xiaobiao Wang*, Kiyoko Miyamoto*, Hidenori Akutsu*, Takahiko Kondo*, Yuji Takahashi*, Tadanobu Ban††, Chizuru Ito¶, Kiyotaka Toshimori¶, Akihiro Nakamura*, Masahiko Ito*, Mami Miyado*, Eisuke Mekada**, and Akihiro Umezawa*

*National Center for Child Health and Development, 2-10-1 Okura, Setagaya, Tokyo 157-8535, Japan; †School of Biomedical Science, Tokyo Medical and Dental University, Yushima, Bunkyo, Tokyo 113-8510, Japan; ¶Graduate School of Medicine, Chiba University, 1-8-1 Inohana, Chuo-ku, Chiba 260-8670, Japan; ‖Center for Developmental Biology, RIKEN Kobe Institute, 2-2-3 Minatojima-minamimachi, Chuo-ku, Kobe, Hyogo 650-0047, Japan; and **Research Institute for Microbial Diseases, and ††Faculty of Medicine, Osaka University, 3-1 Yamadaoka, Suita, Osaka 565-0871, Japan

Edited by Ryuzo Yanagimachi, University of Hawaii, Honolulu, HI, and approved July 8, 2008 (received for review November 8, 2007)

Membrane fusion is an essential step in the encounter of two nuclei from sex cells—sperm and egg—in fertilization. However, aside from the involvement of two molecules, CD9 and Izumo, the mechanism of fusion remains unclear. Here, we show that sperm–egg fusion is mediated by vesicles containing CD9 that are released from the egg and interact with sperm. We demonstrate that the $CD9^{-/-}$ eggs, which have a defective sperm-fusing ability, have impaired release of CD9-containing vesicles. We investigate the fusion-facilitating activity of CD9-containing vesicles by examining the fusion of sperm to $CD9^{-/-}$ eggs with the aid of exogenous CD9-containing vesicles. Moreover, we show, by examining the fusion of sperm to $CD9^{-/-}$ eggs, that hamster eggs have a similar fusing ability as mouse eggs. The CD9-containing vesicle release from unfertilized eggs provides insight into the mechanism required for fusion with sperm.

fertilization | membrane fusion | EGFP | exosome

Fertilization is an essential process that naturally produces a cell capable of developing into a new individual. It consists of sequential events, including membrane fusion of sperm and egg (1). Despite the importance of understanding fertilization in controlling human reproduction and preserving endangered species, the molecular basis underlying the fusion remains a mystery, however. Previously, we reported that a tetraspan-membrane protein (tetraspanin), CD9, is expressed on the egg plasma membrane and is required for sperm–egg fusion (2–4). A role of CD9 in other fusion events also has been demonstrated (5). When sperm are added to eggs from $CD9^{-/-}$ females, the sperm bind to the egg plasma membrane normally, but fusion is severely impaired (2–4). Two recent observations suggest that CD9 plays a role in the organization of egg membrane. First, CD9 is transferred from the egg to the fertilizing sperm present in the perivitelline space (PVS) (6), suggesting the involvement of a process similar to trogocytosis, a mechanism of cell-to-cell contact-dependent transfer of membrane fragments (7). Second, CD9 deficiency alters the length and density of microvilli on the egg plasma membrane (8). CD9 is also known to be a component of exosomes, membrane vesicles released from a wide range of cells (9, 10). Despite its relationship to CD9, the involvement of exosome release in sperm–egg fusion remains unknown. In the present study, we analyzed the potential of enhanced green fluorescent protein (EGFP)-tagged CD9 (CD9-EGFP) as a reporter protein to study sperm–egg fusion in living mouse eggs.

Results

To observe the movement of CD9 during sperm–egg fusion, we generated a transgenic mouse line that expressed CD9-EGFP only in eggs (Fig. 1*A*), and converted to the genetic background of $CD9^{-/-}$ mice by mating mice. Western blot analysis using anti-CD9 monoclonal antibody (mAb) revealed that an expected CD9-EGFP with a molecular mass of 51 kDa (CD9 and EGFP contributing to 24 and 27 kDa, respectively) was expressed in the eggs collected from $Tg^+CD9^{-/-}$ mice; however, the amount of CD9-EGFP expressed in $CD9^{-/-}$ eggs was estimated to be 10% of that of endogenous CD9 in the $CD9^{+/+}$ eggs (Fig. 1*B*). Despite the small amount of CD9-EGFP expressed in eggs, CD9-EGFP demonstrated the ability to reverse the sterility of $CD9^{-/-}$ females (Fig. 1*C*). The numbers of pups obtained from $Tg^+CD9^{-/-}$ females (6.4 ± 0.5) were similar to those from

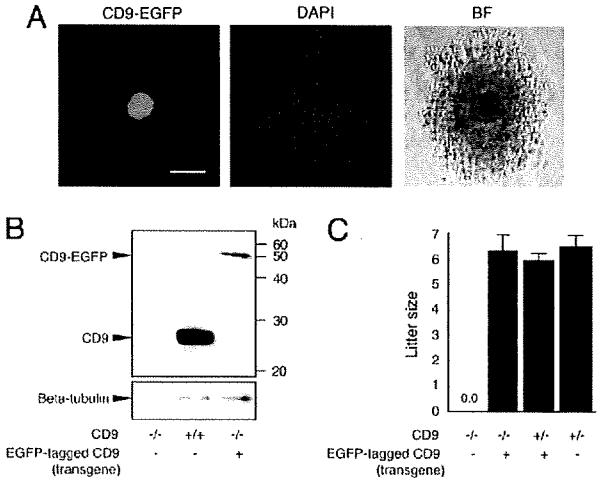

Fig. 1. Generation of mice expressing CD9-EGFP in eggs. (*A*) CD9-EGFP specifically expressed in eggs with mouse ZP3-promoter. Cumulus oocyte complex from $Tg^+CD9^{+/+}$ oviducts was collected at 14 h after injection of human chorionic gonadotropin. Nuclei of an egg and cumulus cells were counterstained with DAPI. (*Left*) CD9-EGFP. (*Center*) DAPI. (*Right*) Bright field. Scale bar: 100 μm. (*B*) Western blot analysis for eggs collected from $CD9^{-/-}$, $CD9^{+/+}$, and $Tg^+CD9^{-/-}$ mice. The same amounts, including 30 eggs of each lysate, were examined by anti-CD9 and anti-beta-tubulin mAbs (internal control). (*C*) Litter sizes of $CD9^{-/-}$ ($n = 31$), $Tg^+CD9^{-/-}$ ($n = 35$), $Tg^+CD9^{+/-}$ ($n = 16$), and $CD9^{+/-}$ mice ($n = 15$) (mean ± SEM). The numbers of females examined are in parentheses.

Author contributions: K. Miyado, K. Yamagata, M.O., and A.U. designed research; K. Miyado, K. Yoshida, K.S., X.W., K. Miyamoto, H.A., T.K., Y.T., T.B., C.I., A.N., M.I., and M.M. performed research; K. Miyado contributed new reagents/analytic tools; K. Miyado, K. Yoshida, H.A., K.T., E.M., and A.U. analyzed data; and K. Miyado wrote the paper.

The authors declare no conflicts of interest.

This article is a PNAS Direct Submission.

Freely available online through the PNAS open access option.

‡K. Miyado and K. Yoshida contributed equally to this work.

§To whom correspondence should be addressed. E-mail: kmiyado@nch.go.jp.

This article contains supporting information online at www.pnas.org/cgi/content/full/0710608105/DCSupplemental.

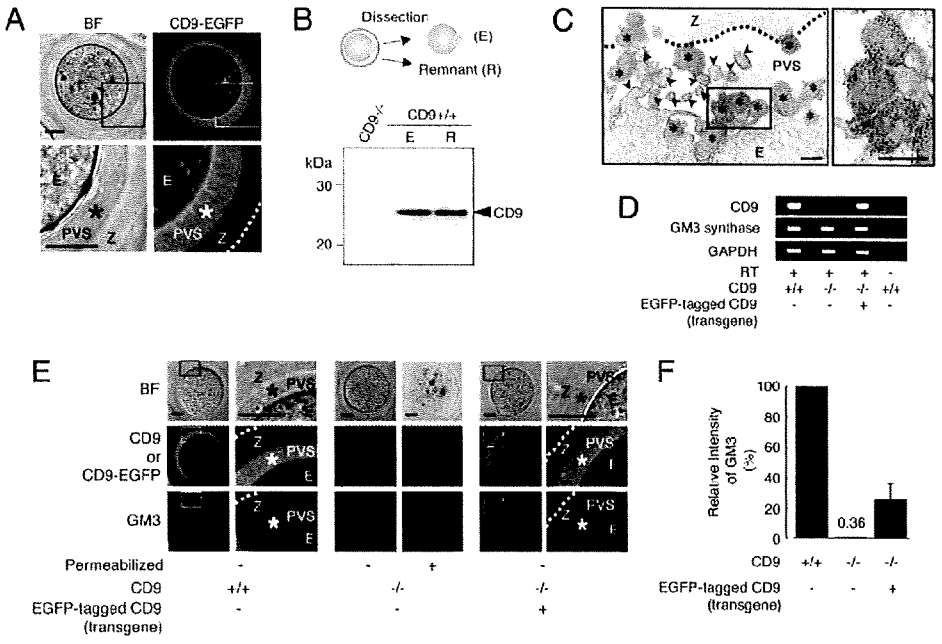

Fig. 2. Identification of secretory vesicles containing CD9 from unfertilized eggs. *A*, A single confocal image showing CD9-EGFP in unfertilized $Tg^+CD9^{-/-}$ eggs (E), including the PVS (*), zona pellucida (Z), and the outer margin of the zona pellucida (dotted line). (*Left*) Bright field. (*Right*) CD9-EGFP. *Lower* are enlarged images of the boxed areas. (*B*) Western blot analysis for eggs mechanically fractionated as shown in the diagram: zona-intact $CD9^{-/-}$ eggs (E) (10 eggs per lane) and zona-free $CD9^{+/+}$ eggs (10 eggs per lane). The medium (R) containing the remnant material from 40 eggs treated with a piezo manipulator was loaded in each lane. (*C*) Immunoelectron-microscopic analysis of $CD9^{+/+}$ eggs. The zona-intact $CD9^{+/+}$ eggs were examined using anti-CD9-mAb and 5-nm gold beads conjugated with anti-rat IgG Ab. Left panel: Image including CD9-containing vesicles (*), microvilli (arrowheads), zona pellucida (Z), perivitelline space (PVS), and egg (E). (*Right*) An enlarged image of the boxed region in the left panel. Scale bar: 200 nm. (*D*) RT-PCR for CD9, GM3 synthase, and glyceraldehyde-3-phosphate dehydrogenase transcripts in $CD9^{+/+}$, $CD9^{-/-}$, and $Tg^+CD9^{-/-}$ eggs. The same amounts, including 50 eggs in each reaction, were examined. The right end lanes are negative controls in which RT was removed from reactions of wild-type eggs. (*E*) Localization of GM3 and CD9 in $CD9^{+/+}$, $CD9^{-/-}$, and $Tg^+CD9^{-/-}$ eggs. (*Left*) Wild-type. (*Middle*) $CD9^{-/-}$. (*Right*) $Tg^+CD9^{-/-}$. Right-side of the sets of wild-type and $Tg^+CD9^{-/-}$ eggs are enlarged images of the boxed regions. The live eggs were examined, and the internal localization of GM3 in $CD9^{-/-}$ eggs was examined under fixed, permeabilized conditions. (*F*) Comparison of the fluorescent intensities of GM3 stained by antibody in wild-type (n = 10), $CD9^{-/-}$ (n = 9), and $Tg^+CD9^{-/-}$ eggs (n = 10) (mean ± SEM). The average values of the wild-type eggs were set to 100%.

$Tg^+CD9^{+/-}$ and $CD9^{+/-}$ females (6.0 ± 0.2 and 6.5 ± 0.5) and greater than those from $CD9^{-/-}$ females (0.0 ± 0.0). The $CD9^{+/-}$ females did not exhibit any loss in fertility that could cause a reduction of litter size relative to that of the $CD9^{+/+}$ females (4). Furthermore, the transgene had no effect on normal fertility. These results demonstrate that transgenically expressed CD9-EGFP can compensate for the loss of intrinsic CD9 and yield eggs with the ability to fuse with sperm.

Based on the foregoing evidence, we observed the subcellular localization of CD9-EGFP in "living" $Tg^+CD9^{-/-}$ eggs (Fig. 2*A*). As expected, confocal microscopic analysis allowed the visualization of two types of CD9-EGFP localization: intense on the plasma membrane and also in the cytoplasm. Unexpectedly, we found loosely filled, noncompacted CD9-EGFP in the PVS, a space formed between the zona pellucida and the plasma membrane of the egg. The localization of CD9 outside the eggs also was confirmed by Western blot analysis using anti-CD9 mAb (Fig. 2*B*). As shown in the diagram, $CD9^{+/+}$ eggs were mechanically fractionated into denuded eggs and other components (R) using a piezo manipulator (11). The fraction R, containing the zona pellucida and the components in the PVS, was centrifuged and subjected to Western blot analysis. The amount of CD9 in the remnant material from 40 eggs was found to be densitometrically equal to that of 10 zona-free eggs, demonstrating an estimated relative abundance of CD9 in the remnant of 20% per egg. Subsequently, we performed immunoelectron-microscopic analysis on the $CD9^{+/+}$ eggs. We identified the vesicles bound to gold particles inside the PVS (Fig. 2*C*). The sectioned microvilli contained a branched network of actin filaments, whereas the variously sized vesicles (50–250 nm in diameter) had uniformly dense materials rather than actin filaments. We also compared $CD9^{+/+}$, $Tg^+CD9^{-/-}$, and $CD9^{-/-}$ eggs by electron-microscopic analysis [supporting information (SI) Fig. S1]. The accumulation of vesicles in the PVS in the $Tg^+CD9^{-/-}$ eggs was comparable to that in the $CD9^{+/+}$ eggs, whereas it was not seen in the $CD9^{-/-}$ or germinal vesicle-staged $CD9^{+/+}$ eggs. These results indicate that 20% of the total amount of CD9 is stored as vesicles in the PVS during meiosis.

We next examined the expression of ganglioside GM3, identified as a CD9-associated molecule (12) and a component of exosomes (10), in $CD9^{+/+}$, $CD9^{-/-}$, and $Tg^+CD9^{-/-}$ eggs. First, we confirmed the expression of GM3 synthase (ST3GalV/SAT-1) (13) in these eggs by RT-PCR (Fig. 2*D*). Then we investigated the localization of GM3 by immunostaining these live eggs with anti-GM3 mAb (Fig. 2*E*). This antibody has been demonstrated to recognize GM3 in the plasma membrane of cells without treatment for permeabilization (14). Finally, we measured the fluorescent intensities of GM3 in these live eggs (Fig. 2*F*). As expected, in wild-type eggs, GM3 was colocalized with CD9 in the PVS and plasma membrane (Fig. 2*E Left* and Fig. 2*F*). In contrast, in $CD9^{-/-}$ eggs, the fluorescent intensities of GM3 were decreased dramatically in the PVS and plasma membrane (0.4% ± 0.2%, relative to 100% for the $CD9^{+/+}$ eggs), consistent with the loss of CD9 (Fig. 2*E Center* and Fig. 2*F*), whereas GM3 could be detected in the cytoplasm of $CD9^{-/-}$ eggs that had been permeabilized by a detergent after fixation. Moreover, the expression of CD9-EGFP reversed the decrease of GM3 in the PVS and plasma membrane of $CD9^{-/-}$ eggs (25.6 ± 10.7%) (Fig. 2*E Right* and Fig. 2*F*), corresponding to the amount of CD9-EGFP quantified by Western blot analysis (Fig. 1*B*). In addition, electron-microscopic analysis revealed that the number of characteristic membrane structures, termed microvilli (1), were significantly decreased in the $CD9^{-/-}$ eggs compared with the $CD9^{+/+}$ eggs (Fig. S2 *A* and *B*). The numbers of microvilli were increased by ≈50% by the expression of CD9-EGFP in the $CD9^{-/-}$ eggs. The analyses of three types of eggs indicate that CD9- and GM3-containing vesicle release is linked to microvilli formation.

We next investigated the involvement of CD9-containing vesicles in sperm–egg fusion (Fig. 3). We found that, based on the length of microvilli (Fig. S2*C*), zona-intact $Tg^+CD9^{-/-}$ eggs can be categorized into two groups (Fig. 3*A*). From single

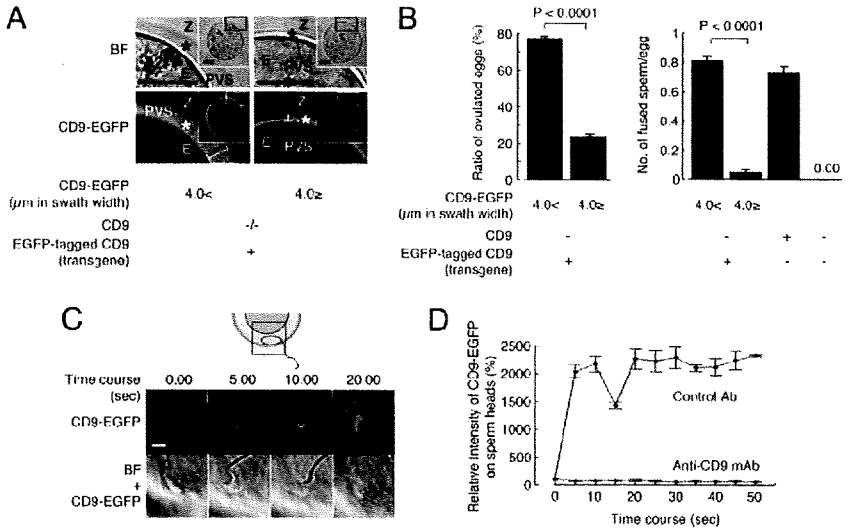

Fig. 3. Involvement of CD9-containing vesicles in sperm–egg fusion. (*A*) Categorization of $Tg^{+}CD9^{-/-}$ eggs (E) into two groups according to the thickness of CD9-EGFP in the PVS (*) and the inner region of the zona pellucida (Z) (>4.0 μm or ≤ 4.0 μm), indicated by double-headed lines. The boxed regions in *Insets* are enlarged. Scale bar: 20 μm. (*B*) Comparison of the fusing ability of two groups of $Tg^{+}CD9^{-/-}$ eggs with wild-type sperm. Left graph: Ratio of two groups of $Tg^{+}CD9^{-/-}$ eggs ovulated from 12 females (mean ± SEM). Right graph: Number of sperm fused per egg in two groups of zona-intact $Tg^{+}CD9^{-/-}$ eggs ovulated from 12 females (>4.0 μm, $n = 204$; ≤4.0 μm, $n = 66$) (mean ± SEM). $CD9^{+/+}$ ($n = 120$) and $CD9^{-/-}$ ($n = 112$) served as positive and negative controls, respectively. (*C* and *D*) Monitoring of the association of egg CD9-containing vesicles with wild-type sperm. $Tg^{+}CD9^{-/-}$ eggs were incubated with the sperm and monitored immediately after the sperm penetrated the zona pellucida under the presence of anti-CD9 mAb (boxed region). The values were calculated from data scanning by confocal microscopy (15 sperm in triplicate dishes) Blue: Preimmune rat IgG. Red: Anti-CD9 mAb (KMC8) (mean ± SEM). The average values of the fluorescent intensities of CD9-EGFP at 0 s were set to 100%, and the final concentration of antibodies was adjusted to 50 μg/ml. Scale bar, 5 μm.

confocal images sectioned through the largest diameter, the accumulation of CD9-EGFP from the plasma membrane to the inner region of the zona pellucida was >4.0 μm in swath width in one group and ≤ 4.0 μm in the other group. The accumulation of CD9-EGFP was predicted to show that CD9-containing vesicles are more highly accumulated within the PVS in the >4.0-μm group compared with the ≤ 4.0-μm group. Comparing the ratio of these two groups in $Tg^{+}CD9^{-/-}$-ovulated eggs revealed a much higher percentage of the >4.0-μm group (77.0 ± 1.3% vs.23.7 ± 1.5%) (Fig. 3*B Left*). Therefore, we focused on the heterogeneity of CD9-EGFP accumulation within the PVS and determined the ratio of the two groups in zona-intact $Tg^{+}CD9^{-/-}$ eggs that successfully fused with the sperm 6 h after insemination. The >4.0-μm group of $Tg^{+}CD9^{-/-}$ eggs showed higher activity for fusion with sperm (0.81 ± 0.04 sperm fused per egg), compared with the ≤40-μm group of $Tg^{+}CD9^{-/-}$ eggs (0.05 ± 0.03) and the $CD9^{-/-}$ eggs (0.00 ± 0.00), and comparable activity to that of wild-type eggs (0.73 ± 0.04) (Fig. 3*B Right*). The average activity of all $Tg^{+}CD9^{-/-}$ eggs (0.72 ± 0.03 sperm fused per egg) was equal to that of wild-type eggs (0.73 ± 0.04 sperm fused per egg). The difference between the two groups of $Tg^{+}CD9^{-/-}$ eggs was statistically significant (Fig. 3*B*). These results suggest that the quantities of CD9-containing vesicles, as assessed by the swath width of CD9-EGFP, are strongly correlated with the frequency of sperm–egg fusion.

To detect the association between sperm and CD9-containing vesicles, we serially monitored the wild-type sperm that penetrated the zona pellucida of the $Tg^{+}CD9^{-/-}$ eggs (Fig. 3 *C* and *D*). As shown in the diagram, we began monitoring the sperm immediately after the head portion of sperm penetrated the zona pellucida of the $Tg^{+}CD9^{-/-}$ eggs (Fig. 3*C Upper*, boxed area in the diagram). Soon after we began to monitor the sperm, the fluorescent intensities of CD9-EGFP on the sperm heads increased and then decreased rapidly between 0 s and 15 s, then increased again, reaching a maximum at 20 s. At this point, the CD9-EGFP fully covered the surface of the sperm heads. In contrast, when the sperm were incubated with $Tg^{+}CD9^{-/-}$ eggs in the medium containing anti-CD9 mAb, no increase in intensity of CD9-EGFP on the sperm heads was detected. Anti-CD9 mAbs have been reported to inhibit sperm–egg fusion (4, 15, 16). Our findings demonstrate that the anti-CD9 mAb inhibited the association of sperm with CD9-containing vesicles in parallel to inhibition of sperm–egg fusion.

To determine whether CD9-containing vesicles are capable of initiating sperm–egg fusion, we incubated the sperm with $CD9^{-/-}$ eggs in medium containing the vesicles collected from $CD9^{+/+}$ eggs (Fig. 4 and Fig. S3). To restrict the source of CD9 into the vesicles from the $CD9^{+/+}$ eggs, we used sperm collected from the epididymis of $CD9^{-/-}$ males. We estimated the capability of the vesicles to influence fusion by counting the number of sperm fused with $CD9^{-/-}$ eggs. As shown in the experimental design, after the zona pellucida was removed from the $CD9^{-/-}$ eggs, the eggs were incubated with sperm in the medium containing the vesicles (Fig. 4*A*). When examined at 1 h after incubation, the sperm were seen to be capable of fusing with $CD9^{-/-}$ eggs after co-incubation with the vesicles (Fig. 4*A Center*), indicating restoration of the fusibility of $CD9^{-/-}$ eggs with the sperm (0.58 ± 0.07 sperm fused per egg) (Fig. 4*B*). We detected further evidence of sperm–egg fusion in the $CD9^{-/-}$ eggs from which a second polar body had been extruded. In contrast, we did not detect improved fusibility of sperm with eggs in medium depleted of CD9-containing vesicles using beads conjugated with anti-CD9 mAb (Fig. 4*A Right* and *B*). After treatment with the beads, the quantity of CD9 in the depleted medium was significantly decreased, to 16% of the untreated medium (Fig. 4*C*). In addition, $CD9^{-/-}$ remnants failed to rescue the fusing ability of $CD9^{-/-}$ eggs. These findings indicate that the association with CD9-containing vesicles renders the sperm capable of fusing with eggs without endogenous CD9 expression. We estimated the relative abundance of CD9 in the remnant as 18% of the total amount in the eggs (Fig. 4*C*). We further found

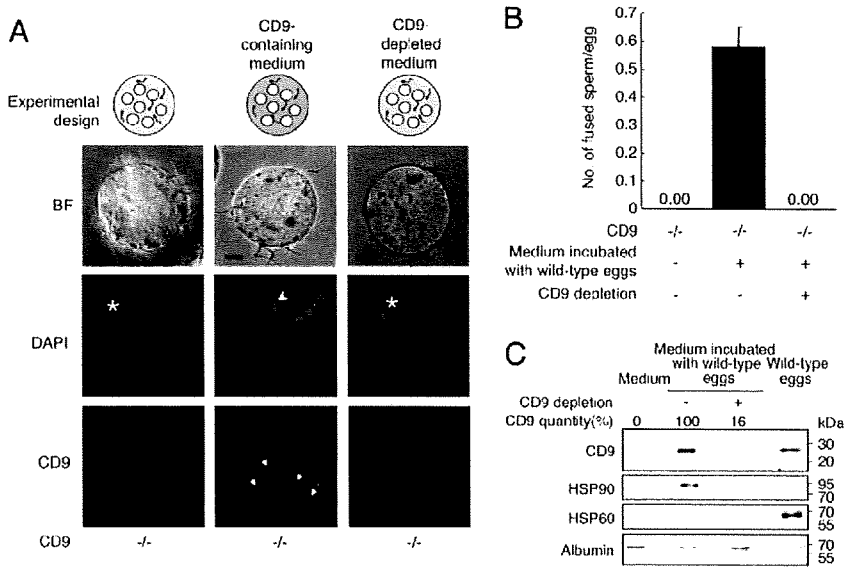

Fig. 4. Identification of fusion-facilitating activity of CD9-containing vesicles. (*A*) Estimation of the fusion-facilitating ability of the vesicles in sperm–egg fusion. As shown in the experimental design, $CD9^{-/-}$ sperm were incubated with $CD9^{-/-}$ eggs (white circles) in media containing egg-released vesicles after the zona pellucida was removed from these eggs. CD9 was detected by anti-CD9 mAb conjugated with Alexa488. The eggs were preloaded with DAPI before incubation with the sperm, to allow counting of the number of fused sperm. (*Left*) $CD9^{-/-}$ eggs at 1 h after incubation with the sperm, as a negative control. *Center* $CD9^{-/-}$ eggs cultured in the medium containing CD9 collected from wild-type eggs. (*Right*) $CD9^{-/-}$ eggs cultured in the medium depleted of CD9 by beads conjugated with anti-CD9 mAb, showing the fused sperm to eggs (arrowhead), metaphase II–arrested chromosomes (*), a second polar body (open arrowhead), and CD9 translocated on the sperm heads (arrow). The fluorescent z-series images were projected as three-dimensional images. Scale bar: 20 μm. (*B*) Number of fused sperm with the zona-free eggs counted at 1 h after incubation (mean ± SEM): $CD9^{-/-}$ eggs as a negative control ($n = 51$), $CD9^{-/-}$ eggs cultured in the medium containing CD9 ($n = 112$), and $CD9^{-/-}$ eggs cultured in the medium depleted of CD9 by antibody-conjugated beads ($n = 74$). The total numbers of eggs examined are in parentheses. (*C*) Western blot analysis of the media incubated with $CD9^{+/+}$ eggs for CD9, HSP90, and HSP60. Loaded samples (left to right): The medium as a negative control, the medium containing the remnant material from 40 eggs per lane (bead-untreated and -treated), and 5 eggs per lane as a positive control. The albumin contained in the medium was detected by Coomassie brilliant blue staining as an internal control. The quantities of CD9 in the media were measured densitometrically (using National Institutes of Health Image software).

that the decreased amount of CD9 after the bead treatment was synchronized with that of a cytoplasmic chaperone, HSP90 (17), but not with a mitochondrial chaperone, HSP60 (18). Our analysis of the egg-conditioned medium indicated that CD9-containing vesicles contained HSP90, a conserved component of exosomes (9, 10).

To estimate the contribution of CD9-containing vesicles to sperm–egg fusion, we examined the restoration of the impaired sperm-fusing ability in $CD9^{-/-}$ eggs co-incubated with $CD9^{+/-}$ or $CD9^{+/+}$ eggs expressing endogenous CD9 (Figs. 5 and S4*A*). We predicted that when sperm were incubated with a mixture of eggs, the vesicles released from $CD9^{+/-}$ or $CD9^{+/+}$ eggs would

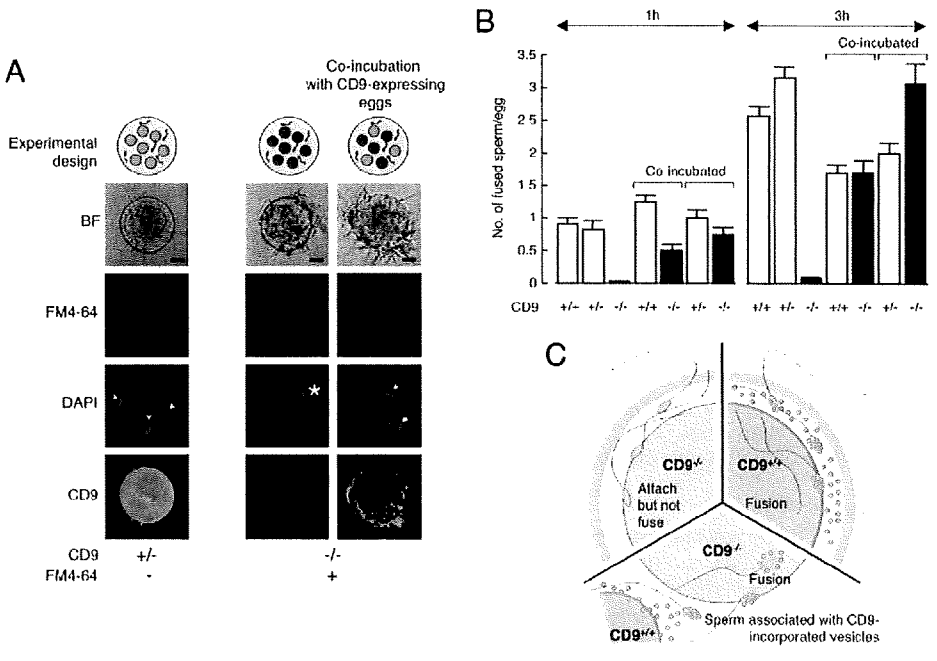

Fig. 5. Recovery of impaired fusion of $CD9^{-/-}$ eggs with sperm by CD9-containing vesicles. (*A*) Estimation of the fusion-facilitating ability of the vesicles in sperm–egg fusion. As shown in the experimental design, sperm were incubated with a mixture of CD9-expressing eggs (green circles) and $CD9^{-/-}$ eggs (red circles) after the zona pellucida was removed from these eggs. The eggs were preloaded with DAPI before incubation with sperm, to allow counting of the number of fused sperm. $CD9^{-/-}$ eggs were prestained with FM4–64 and thus were easily distinguished from CD9-expressing eggs after incubation with the sperm. (*Left*) $CD9^{+/-}$ eggs at 1 h after incubation with the sperm, as a positive control. (*Center*) $CD9^{-/-}$ eggs, as a negative control. (*Right*) $CD9^{-/-}$ eggs co-incubated with $CD9^{+/-}$ eggs, showing fused sperm to egg (arrowheads), metaphase II–arrested chromosomes (*), and extruded second polar body (arrow). The fluorescent z-series images were projected as three-dimensional images. CD9 was detected by anti-CD9 mAb conjugated with Alexa488. Scale bar: 20 μm. (*B*) Numbers of fused sperm with the zona-free eggs counted at 1 and 3 h after incubation (mean ± SEM). $CD9^{+/-}$ (1 h: $n = 34$; 3 h: $n = 55$), $CD9^{+/+}$ (1 h: $n = 71$; 3 h: $n = 79$), and $CD9^{-/-}$ eggs (1 h: $n = 100$; 3 h: $n = 115$) were separately incubated with sperm. Total number of coincubated eggs examined: $CD9^{+/-}$ eggs ($n = 54$) coincubated with $CD9^{-/-}$ eggs ($n = 60$), and $CD9^{+/+}$ eggs ($n = 65$) coincubated with $CD9^{-/-}$ eggs ($n = 74$) at 1 h; $CD9^{+/-}$ eggs ($n = 51$) coincubated with $CD9^{-/-}$ eggs ($n = 33$), and $CD9^{+/+}$ eggs ($n = 98$) coincubated with $CD9^{-/-}$ eggs ($n = 90$) at 3 h. (*C*) Schematic model of involvement of CD9-containing vesicles in sperm–egg fusion: $CD9^{+/+}$ (green), $CD9^{-/-}$ (light blue), and $CD9^{-/-}$ eggs coincubated with $CD9^{+/+}$ wild-type eggs with sperm (yellow).

interact with sperm, and these sperm could fuse with $CD9^{-/-}$ eggs. If sperm-fusing ability were regulated mainly by CD9-containing vesicles, then the number of sperm fused to $CD9^{-/-}$ eggs would be predicted to be almost equal to that fused to $CD9^{+/-}$ or $CD9^{+/+}$ eggs coincubated with $CD9^{-/-}$ eggs. We counted the number of fused sperm in coincubated CD9-expressing eggs ($CD9^{+/-}$ and $CD9^{+/+}$) and $CD9^{-/-}$ eggs. The $CD9^{-/-}$ eggs were prestained with FM4–64 (19), a fluorescent dye used to stain the membrane of live cells, and thus could be easily distinguished from the $CD9^{+/-}$ and $CD9^{+/+}$ eggs. FM4–64 did not transfer between the $CD9^{-/-}$ eggs and the $CD9^{+/-}$ or $CD9^{+/+}$ eggs. As shown in the experimental design, after the zona pellucida was removed from the eggs, $CD9^{-/-}$ eggs (red circles) were mixed with $CD9^{+/-}$ or $CD9^{+/+}$ eggs (green circles), and sperm were added to the medium containing these eggs (Fig. 5*A*). At 1 h after insemination, significant fusion of sperm with the $CD9^{-/-}$ eggs was facilitated (0.75 ± 0.11 and 0.50 ± 0.09 sperm fused per egg), corresponding to that in the $CD9^{+/-}$ (1.00 ± 0.13) and $CD9^{+/+}$ eggs (1.25 ± 0.10). At 3 h after insemination, the fusion of sperm with the $CD9^{-/-}$ eggs was restored (3.06 ± 0.30 and 1.70 ± 0.18 sperm fused per egg) to levels comparable to those in the $CD9^{+/-}$ (2.00 ± 0.15) and $CD9^{+/+}$ eggs (1.69 ± 0.13). We also detected a second polar body extruding from the $CD9^{-/-}$ eggs (Fig. 5*A Right*, arrow). In contrast, we did not observe the translocation of vesicles from the $CD9^{+/-}$ and $CD9^{+/+}$ eggs to the $CD9^{-/-}$ eggs when sperm were not added to the mixture, even after 10 h of incubation (Fig. S4*B*). These data demonstrate that the defect in the fusing ability of $CD9^{-/-}$ eggs is caused by dysfunction of the mechanism facilitating the sperm-fusing activity through CD9-containing vesicles.

To further study the involvement of CD9-containing vesicles in regulating sperm-fusing ability, we evaluated the capability of hamster eggs in sperm–egg fusion (Fig. S5). Hamster eggs have the ability to fuse with other mammalian sperm and thus are used as a tool to evaluate the fusing ability of human sperm (20). When hamster eggs were incubated with $CD9^{-/-}$ eggs after the zona pellucida was removed from these eggs, the sperm-fusing ability of these eggs was improved significantly. The sperm-fusing ability acquired through the exposure to hamster eggs was not as great as that produced by exposure to mouse eggs, probably due to the slightly different CD9 in hamster and mouse eggs (21). These results indicate that the function of CD9-containing vesicles in the acquisition of sperm-fusing ability is widely conserved in mammals.

Discussion

In sperm–egg fusion, there is a significant direct interaction between the cell membranes of sperm and eggs (1, 20, 22); however, our results demonstrate that CD9-containing vesicle–sperm interaction precedes the direct cell membrane interaction between sperm and eggs. Based on our data, we propose that the release of CD9-containing vesicles from eggs before fertilization facilitates the sperm-fusing ability that renders the sperm competent to fuse with $CD9^{-/-}$ eggs (Fig. 5*C*). Our finding of CD9-EGFP in living unfertilized eggs demonstrates that CD9-containing vesicles are present in the PVS, and that these vesicles accumulate inside the PVS during the germinal vesicle (1) and metaphase II-arrested stages (1). During this period, the egg undergoes drastic cytological changes with the increased number of microvilli (1, 22), predicting the correlation between vesicle release and microvilli formation. As expected, this correlation is supported by the finding that CD9 deficiency leads not only to impaired microvilli formation (8) (Fig. S2), but also to decreased accumulation of vesicles within the PVS. These data support the association between the release of CD9-containing vesicles from eggs and the formation of microvilli on the egg plasma membrane.

As reported previously, somatic cells are capable of releasing proteins and lipids included in membrane organelles, termed exosomes (9, 10), which are pinched out from the plasma membrane (23). Exosomes share many additional properties with retroviral particles, including similar lipid and protein compositions, such as tetraspanin (23). GM3 and HSP90 are known to be conserved components of exosomes (10). Our results show that CD9-containing vesicles released from eggs share these two components, implying that the vesicles are "exosome-like." Previous studies of macrophages have proposed that exosome biogenesis occurs only by outward budding at endosomal membranes, followed by the fusion of vesicle-laden endosomes with the plasma membrane (9, 23). If the CD9-containing vesicle were derived from exosomes and generated from the fusion of endosomes with the plasma membrane, then the vesicles would contain some proteases (9, 23), fuse with the sperm membrane, and possibly activate the sperm fusogenic factor(s) by enzymatic activities.

In hamster eggs, expansion of the PVS has been deemed essential or at least beneficial to normal fertilization (20, 21, 24), indicating that materials involved in fusion with sperm are released from eggs before fertilization in hamsters and in mice. Because anti-CD9 mAbs are not available for hamster CD9, we could not directly confirm CD9-containing vesicle release from hamster eggs before fertilization. Instead, our co-incubation assay demonstrated that hamster eggs facilitate the fusion of sperm with $CD9^{-/-}$ eggs, indicating that hamster eggs share a similar mechanism with mouse eggs through egg-released materials. Moreover, it has been reported that growing oocytes bind to sperm and transfer fluorescent dyes to the sperm head (25). At this stage, oocytes have CD9 on the cell membrane but lack CD9-containing vesicles (Fig. S1). We presume that the transfer of fluorescent dye from growing oocytes to sperm heads is mediated by CD9 on the cell membrane. Based on our findings, we propose that the CD9-containing vesicle has an ability to facilitate sperm—egg fusion. This knowledge has great potential for clinical applications, such as the induction of sperm–egg fusion using exogenous sources.

Materials and Methods

Animals. The mice that we produced were back-crossed into a C57BL/6 genetic background. Wild-type eggs were collected from C57BL/6 females (8–12 weeks old). Wild-type sperm were obtained from the epididymides of B6C3F1 males (8–12 weeks old). Hamster eggs were obtained commercially as frozen unfertilized eggs (NOSAN).

Antibodies and Chemicals. Antibodies against CD9 (KMC; BD PharMingen), beta-tubulin (Tub2.1; Sigma), HSP60 (24/HSP60; BD PharMingen), HSP90 (16F1; MBL), and GM3 (GMR6; Seikagaku) were used. Antibodies labeled with biotin by a labeling kit (Dojindo) and horseradish peroxidase-conjugated streptavidin (Sigma) were used for Western blot analysis. For immunostaining, antibodies were labeled directly with Alexa488 and Alexa546 using labeling kits (Invitrogen). FM4–64 (Invitrogen) was used to define the lipid bilayer of live eggs without disturbing sperm–egg fusion (10 μM at final concentration). We used DAPI (Invitrogen), a fluorescent dye that slowly permeates the living cell membrane (semipermeable) and slowly leaks out of cells after washing relative to Hoechst33342 (permeable), in counting the number of sperm fused per egg.

Transgenic Mice. The construct expressing mouse CD9 tagged at the N terminus with EGFP (CD9-EGFP) was subcloned into plasmid DNA-containing mouse ZP3 promoter (26). The expression cassette was excised by restriction enzyme digestion and microinjected into fertilized eggs of C57BL/6 mice, according to standard techniques (27).

Genotyping and RT-PCR. Mouse genotyping and RT-PCR were performed following standard procedures (27). (Primer sets are listed in Table S1).

Egg Collection. Eggs were collected from the oviduct 14–16 h after human chorionic gonadotropin injection (4). The eggs were placed in a drop of TYH

medium (28). Sperm collected from the epididymides were capacitated in a 100-μl drop of medium. The eggs were incubated with 1.5×10^5 sperm/ml at 37°C in 5% CO_2, and unbound sperm were washed away. The zona pellucida was removed from the eggs with acidic Tyrode's solution (4) or a piezo manipulator (11). A hole was punched through the zona pellucida with a piezo manipulator, and the eggs were removed. All materials were aspirated, including the medium but not the eggs, and used as "remnants."

Immunostaining. Zona-intact live eggs were stained with diluted antibodies in TYH medium for 30 min at 37°C, and the nonspecifically accumulated antibodies in the PVS were washed away after a brief incubation (30 min) in the medium. To measure the fluorescent intensities of GM3, three types of eggs were stained by Alexa546-labeled anti-GM3 mAb in TYH medium for 30 min, then washed in the medium for 30 min. Staining was visualized using a laser scanning confocal microscope (LSM 510 META; Carl Zeiss).

Electron-Microscopic Analysis. Live eggs were incubated with anti-CD9 mAb and anti-rat IgG mAb tagged with 5-nm gold beads. After incubation, the eggs were fixed by glutaraldehyde and osmic acid solutions. Ultra-thin sections were prepared as described in ref. 29. Eggs denuded with acid Tyrode's solution were fixed with a mixture of paraformaldehyde and glutaraldehyde and osmic acid solutions.

***In Vitro* Fertilization.** To observe the fusion with the sperm, zona-intact and zona-free eggs were incubated with DAPI (10 μg/ml) in the medium for 20 min, then washed before the sperm were added. This procedure allowed the staining of only fused sperm nuclei by dye-transfer into sperm after membrane fusion. At 1 h or 3 h after incubation in a 30-μl drop of medium, the eggs were fixed with a mixture of paraformaldehyde and glutaraldehyde for 20 min at 4°C.

Monitoring the Association of CD9-Containing Vesicles with Sperm. Eggs collected from $Tg^+CD9^{-/-}$ females were set in a 30-μl drop of TYM medium. The sperm were added to the eggs at a final concentration of 1.5×10^5/ml after incubation in the medium for 2 h. Posts of latex beads were deposited around the eggs. A glass coverslip was carefully pressed down onto the posts until the egg were fixed. The medium containing eggs and sperm was cooled to 10°C before observation. Cooling reduced the sperm motility. This procedure allowed us to measure the CD9-EGFP fluorescence on the sperm head using a confocal microscope. Images of the sperm were captured at 1 frame/s. The average value of the fluorescent intensities of CD9-EGFP at 0 s was set to 100%, and the final concentration of antibodies was adjusted to 50 μg/ml. The data are measurements of serial images from 15 wild-type sperm in triplicate dishes.

Collection of CD9-Containing Vesicles. The medium containing the vesicles was collected from denuded wild-type eggs. The eggs were cultured in a 60-μl drop of medium for 2 h after the zona pellucida was removed from the eggs. Collecting the medium containing the vesicles required an incubation time of 2 h. The collected medium was used for analysis of vesicle components and evaluation of sperm-fusing ability. CD9-depleted medium was used as a negative control. After the zona pellucida was removed from $CD9^{-/-}$ eggs, the eggs were incubated with the sperm in the medium containing CD9-incorporated vesicles for 1 h, for comparison with the vesicle-depleted medium. Details are shown in Fig. S3.

Western Blot Analysis. Quantities of proteins were examined by Western blot analysis, as described in ref. 4. As an internal loading control, quantities of albumin included in the medium were examined using Coomassie brilliant blue staining. Details are shown in Fig. S3.

Coincubation of Two Types of Eggs. $CD9^{-/-}$ eggs and CD9-expressing eggs ($CD9^{+/-}$ and $CD9^{+/+}$) were incubated in each 30-μl drop of medium after the zona pellucida was removed from these eggs. At 2 h after incubation, the $CD9^{-/-}$ eggs were added into the cultured medium of the CD9-expressing eggs. Sperm were added into the medium containing two types of eggs and incubated for 1 or 3 h. Details are shown in Fig. S4A. The frozen hamster eggs also were incubated with the $CD9^{-/-}$ eggs and wild-type sperm for 1 h. The zona pellucida of frozen hamster eggs was hardened, and removing the zona pellucida using acid Tyrode's solution took 5 min. Details are shown in Fig. S5A.

ACKNOWLEDGMENTS. This work was supported by a Precursory Research for Embryonic Science and Technology (PRESTO) grant from the Japanese Ministry of Health, Labor and Welfare and by a Grant-in-Aid for Scientific Research from the Japanese Ministry of Education, Culture, Sports, and Technology.

1. Yanagimachi R (1994) in *The Physiology of Reproduction*, eds Knobil E, Neill JD (Raven, New York), pp 189–317.
2. Kaji K, *et al.* (2000) The gamete fusion process is defective in eggs of Cd9-deficient mice. *Nat Genet* 24:279–282.
3. Le Naour F, Rubinstein E, Jasmin C, Prenant M, Boucheix C (2000) Severely reduced female fertility in CD9-deficient mice. *Science* 287:319–321.
4. Miyado K, *et al.* (2000) Requirement of CD9 on the egg plasma membrane for fertilization. *Science* 287:321–324.
5. Hemler ME (2003) Tetraspanin proteins mediate cellular penetration, invasion, and fusion events and define a novel type of membrane microdomain. *Annu Rev Cell Dev Biol* 19:397–422.
6. Barraud-Lange V, Naud-Barriant N, Bomsel M, Wolf J-P, Ziyyat A (2007) Transfer of oocyte membrane fragments to fertilizing spermatozoa. *FASEB J* 21:3446–3449.
7. Joly E, Hudrisier D (2003) What is trogocytosis and what is its purpose? *Nat Immunol* 4:815.
8. Runge K-E, *et al.* (2007) Oocyte CD9 is enriched on the microvillar membrane and required for normal microvillar shape and distribution. *Dev Biol* 304:317–325.
9. Traikovic K, *et al.* (2008) Ceramide triggers budding of exosome vesicles into multivesicular endosomes. *Science* 319:1244–1247.
10. Wubbolts R, *et al.* (2003) Proteomic and biochemical analyses of human B cell-derived exosomes: Potential implications for their function and multivesicular body formation. *J Biol Chem* 278:10963–10972.
11. Yamagata K, *et al.* (2002) Sperm from the calmegin-deficient mouse have normal abilities for binding and fusion to the egg plasma membrane. *Dev Biol* 250:348–357.
12. Mitsuzuka K, Handa K, Satoh M, Arai Y, Hakomori S (2005) A specific microdomain ("glycosynapse 3") controls phenotypic conversion and reversion of bladder cancer cells through GM3-mediated interaction of alpha3beta1 integrin with CD9. *J Biol Chem* 280:35545–35553.
13. Yamashita T, *et al.* (2003) Enhanced insulin sensitivity in mice lacking ganglioside GM3. *Proc Natl Acad Sci USA* 100:3445–3449.
14. Kotani M, Ozawa H, Kawashima I, Ando S, Tai T (1992) Generation of one set of monoclonal antibodies specific for a-pathway ganglio-series gangliosides. *Biochim Biophys Acta* 1117:97–103.
15. Chen MS, *et al.* (1999) Role of the integrin-associated protein CD9 in binding between sperm ADAM 2 and the egg integrin alpha6beta 1: Implications for murine fertilization. *Proc Natl Acad Sci USA* 96:11830–11835.
16. Miller B-J, Georges-Labouesse E, Primakoff P, Myles D-G (2000) Normal fertilization occurs with eggs lacking the integrin alpha6beta1 and is CD9-dependent. *J Cell Biol* 149:1289–1296.
17. Callahan M-K, Garg M, Srivastava P-K (2008) Heat-shock protein 90 associates with N-terminal extended peptides and is required for direct and indirect antigen presentation. *Proc Natl Acad Sci USA* 105:1662–1667.
18. Cheng M-Y, Hartl F-U, Horwich A-L (1990) The mitochondrial chaperonin hsp60 is required for its own assembly. *Nature* 348:455–458.
19. Bolte S, *et al.* (2004) FM-dyes as experimental probes for dissecting vesicle trafficking in living plant cells. *J Microsc* 214:159–173.
20. Yanagimachi R, Yanagimachi H, Rogers B-J (1976) The use of zona-free animal ova as a test system for the assessment of the fertilizing capacity of human spermatozoa. *Biol Reprod* 15:471–476.
21. Ponce R-H, Yanagimachi R, Urch U-A, Yamagata T, Ito M (1993) Retention of hamster oolemma fusibility with spermatozoa after various enzyme treatments: A search for the molecules involved in sperm–egg fusion. *Zygote* 1:163–171.
22. Primakoff P, Myles D-G (2002) Penetration, adhesion, and fusion in mammalian sperm–egg interaction. *Science* 296:2183–2185.
23. Booth A-M, *et al.* (2006) Exosomes and HIV *Gag* bud from endosome-like domains of the T cell plasma membrane. *J Cell Biol* 172:923–935.
24. Okada A, Yanagimachi R, Yanagimachi H (1986) Development of a cortical granule-free area of cortex and the perivitelline space in the hamster oocyte during maturation and following ovulation. *J Submicrosc Cytol* 18:233–247.
25. Zuccotti M, Yanagimachi R, Yanagimachi H (1991) The ability of hamster oolemma to fuse with spermatozoa: Its acquisition during oogenesis and loss after fertilization. *Development* 112:143–152.
26. Rankin T-L, *et al.* (1998) Human ZP3 restores fertility in Zp3 null mice without affecting order-specific sperm binding. *Development* 125:2415–2424.
27. Hogan B, Costantini F, Lacy E (1986) in *Manipulating the Mouse Embryo* (Cold Spring Harbor Lab Press, Cold Spring Harbor, NY), pp 217–252.
28. Toyoda Y, Chang M-C (1974) Capacitation of epididymal spermatozoa in a medium with high K-Na ratio and cyclic AMP for the fertilization of rat eggs in vitro. *J Reprod Fertil* 36:125–134.
29. Toshimori K, Saxena D-K, Tanii I, Yoshinaga K (1998) An MN9 antigenic molecule, equatorin, is required for successful sperm–oocyte fusion in mice. *Biol Reprod* 59:22–29.

THE JOURNAL OF BIOLOGICAL CHEMISTRY VOL. 283, NO. 38, pp. 26089–26097, September 19, 2008

Double Deficiency of Tetraspanins CD9 and CD81 Alters Cell Motility and Protease Production of Macrophages and Causes Chronic Obstructive Pulmonary Disease-like Phenotype in Mice*[S]

Received for publication, March 10, 2008, and in revised form, July 7, 2008 Published, JBC Papers in Press, July 28, 2008, DOI 10.1074/jbc.M801902200

Yoshito Takeda[‡1], Ping He[‡§1], Isao Tachibana[‡2], Bo Zhou[‡], Kenji Miyado[¶3], Hideshi Kaneko[‖], Mayumi Suzuki[‡], Seigo Minami[‡], Takeo Iwasaki[‡], Sho Goya[‡], Takashi Kijima[‡], Toru Kumagai[‡], Mitsuhiro Yoshida[‡], Tadashi Osaki[‡], Toshihisa Komori[‡4], Eisuke Mekada[¶], and Ichiro Kawase[‡]

From the [‡]Department of Respiratory Medicine, Allergy and Rheumatic Diseases, Osaka University Graduate School of Medicine, Osaka 565-0871, Japan, the [§]Department of Respiratory Medicine, the Second Affiliated Hospital, School of Medicine, Xi'an Jiaotong University, Xi'an, 71004 China, [¶]Research Institute for Microbial Diseases, Osaka University, Osaka 565-0871, Japan, and [‖]Pharmacological and Safety Research Department, Pharmaceutical Development Research Laboratories, Teijin Pharma Limited, Tokyo 191-8512, Japan

CD9 and CD81 are closely related tetraspanins that regulate cell motility and signaling by facilitating the organization of multimolecular membrane complexes, including integrins. We show that CD9 and CD81 are down-regulated in smoking-related inflammatory response of a macrophage line, RAW264.7. When functions of CD9 and CD81 were ablated with monoclonal antibody treatment, small interfering RNA transfection, or gene knock-out, macrophages were less motile and produced larger amounts of matrix metalloproteinase (MMP)-2 and MMP-9 than control cells *in vitro*. In line with this, CD9/CD81 double-knock-out mice spontaneously developed pulmonary emphysema, a major pathological component of chronic obstructive pulmonary disease (COPD). The mutant lung contained an increased number of alveolar macrophages with elevated activities of MMP-2 and MMP-9 and progressively displayed enlarged airspace and disruption of elastic fibers in the alveoli. Secretory cell metaplasia, a finding similar to goblet cell metaplasia in cigarette smokers, was also observed in the epithelium of terminal bronchioles. With aging, the double-knock-out mice showed extrapulmonary phenotypes, including weight loss, kyphosis, and osteopenia. These results suggest that the tetraspanins CD9 and CD81 regulate cell motility and protease production of macrophages and that their dysfunction may underlie the progression of COPD.

Chronic obstructive pulmonary disease (COPD),[5] a disease defined by incompletely reversible airflow limitation, results from abnormal inflammatory response to chronic cigarette smoking. Pulmonary emphysema is a major component of COPD, and a dominant hypothesis in its pathophysiology is that persistent infiltration of inflammatory cells and production of proteases, including matrix metalloproteinases (MMPs) in the lung, lead to tissue destruction and airspace enlargement (1, 2). In patients with emphysema, there was an increase in bronchoalveolar lavage fluid (BALF) concentrations and macrophage expression of MMP-9 (3). Studies of human samples have shown increases of MMP-2 and MMP-9 in smoking-related emphysema (4). Alveolar macrophages secrete elastolytic enzymes, including MMP-2, MMP-9, and MMP-12, and play a pivotal role in the pathophysiology of COPD. There was a marked increase in the numbers of macrophages in airways, lung parenchyma, BALF, and sputum in patients with emphysema (2). Macrophages are activated by cigarette smoke to release inflammatory mediators such as TNF-α, chemokines, and reactive oxygen species as well as MMPs, providing a cellular mechanism that links smoking with inflammation in COPD (2). It was recently proposed that lowered activity of histone deacetylases (HDACs), which are suppressors of inflammatory genes, accounts for the persistent activation of macrophages in COPD patients (5).

The tetraspanin proteins include at least 33 members, including CD9, CD63, CD81, CD82, and CD151 in mammals. They are characterized by the structure that spans the plasma membrane four times and have a propensity to form complexes with each other and with other functional molecules, including

* This work was supported by a grant from Takeda Science Foundation, Osaka, Japan (to I. T.), and a grant from "Kansai Biomedical Cluster" Project in Saito, Japan, which is promoted by the Knowledge Cluster Initiative of the Ministry of Education, Culture, Sports, Science and Technology, Japan (to I. T.). The costs of publication of this article were defrayed in part by the payment of page charges. This article must therefore be hereby marked "*advertisement*" in accordance with 18 U.S.C. Section 1734 solely to indicate this fact.

[S] The on-line version of this article (available at http://www.jbc.org) contains supplemental Experimental Procedures, Figs. 1–4, Tables 1 and 2, and Video 1.

[1] Both authors contributed equally to this work.

[2] To whom correspondence should be addressed: Dept. of Respiratory Medicine, Allergy and Rheumatic Diseases, Osaka University Graduate School of Medicine, Osaka 565-0871, Japan. Tel.: 81-6-6879-3833; Fax: 81-6-6879-3839; E-mail: itachi02@imed3.med.osaka-u.ac.jp.

[3] Present address: Dept. of Reproductive Biology and Pathology, National Center for Child Health and Development, Tokyo 157-8535, Japan.

[4] Present address: Division of Cell Biology, Dept. of Basic Medical Sciences, Nagasaki University Graduate School of Biomedical Sciences, Nagasaki 852-8588, Japan.

[5] The abbreviations used are: COPD, chronic obstructive pulmonary disease; MMP, matrix metalloproteinase; BALF, bronchoalveolar lavage fluid; HDAC, histone deacetylase; KO, knock-out; DKO, double-knock-out; TSA, trichostatin A; CSE, cigarette smoke extract; TIMP, tissue inhibitor of metalloproteinase; FN, fibronectin; BMDM, bone marrow-derived macrophage; pQCT, peripheral quantitative computed tomography; IFN, interferon; mAb, monoclonal antibody; siRNA, small interfering RNA; DMEM, Dulbecco's modified Eagle's medium; FBS, fetal bovine serum; WT, wild type; RT, reverse transcription; TNF-α, tumor necrosis factor-α; PAS, periodic acid-Schiff.

integrins, signaling proteins, and membrane-anchored growth factors at specialized membrane microdomains. As organizer of these multimeric complexes, tetraspanins regulate cell morphology, motility, invasion, fusion, and signaling (6). It has been increasingly recognized that tetraspanin-integrin complexes also regulate the production of MMPs, particularly in tumor cells. Treatment of a breast cancer cell line with anti-tetraspanin monoclonal antibodies (mAbs) stimulated production of MMP-2 and formation of invasive protrusions (7). CD9 expression inhibited integrin-dependent morphologic differentiation and MMP-2 production of small cell lung cancer cells via the phosphatidylinositol 3-kinase/Akt pathway (8). Overexpression of CD81 or CD82 reduced cell motility and MMP-9 activity in multiple myeloma cell lines (9). However, their role in motility and MMP production of macrophage has yet to be studied.

In this study, our *in vitro* experiments show that CD9 and CD81, the two widely distributed and closely correlated tetraspanins, are down-regulated in smoking-related inflammatory response of macrophages and that ablation of their function suppresses cell motility and increases the production of MMPs. Moreover, *in vivo* experiments using CD9/CD81 double-knock-out (DKO) mice displayed accumulation of macrophages and increased activities of MMPs in the mutant lung. The DKO mice progressively developed pulmonary emphysema, weight loss, and osteopenia, a phenotype akin to human COPD.

EXPERIMENTAL PROCEDURES

Immunoblotting—A mouse macrophage line, RAW264.7, and a human alveolar epithelial cell line, A549, were serum-starved for 24 h and treated with 10 ng/ml trichostatin A (TSA; Wako Pure Chemical Industries, Osaka, Japan) or 0.1% cigarette smoke extract (CSE) as described previously (10) for 48 h. In some experiments, 10 μM theophylline (Wako Pure Chemical Industries) or 1 μM dexamethasone (Sigma) were co-added with TSA into the culture. Cells were lysed in lysis buffer containing 1% Brij99, 25 mM HEPES (pH 7.5), 150 mM NaCl, 5 mM $MgCl_2$, 2 mM phenylmethylsulfonyl fluoride, 10 μg/ml aprotinin, and 10 μg/ml leupeptin. Cell lysates were separated by SDS-PAGE, transferred to polyvinylidene difluoride membranes, and probed with rat anti-mouse CD9 (KMC8) and integrin β1 (KMI6) mAbs (BD Biosciences) and hamster anti-mouse CD81 mAb (Eat2; AbD Serotec, Oxford, UK). For A549 lysates, mouse anti-human CD9 (MM2/57; BIOSOURCE) and CD81 (JS64; Immunotech, Marseille, France) mAbs were used.

Treatment of RAW264.7 Cells with mAbs or Small Interfering RNA (siRNA) Transfection against CD9 and CD81—To test the effects of function-inhibitory mAbs to CD9 (KMC8) and CD81 (2F7; Southern Biotechnology, Birmingham, AL), RAW264.7 cells were cultured in DMEM containing 0.1% FBS for 24 h in the absence or presence of 20 μg/ml of IgG (isotype matched with KMC8), KMC8, 2F7, and KMC8 plus 2F7. mRNA was extracted, and expressions of MMP-2, MMP-9, MMP-12, tissue inhibitor of metalloproteinase (TIMP)-1, and TIMP-2 were evaluated by reverse transcription (RT)-PCR as described previously (11, 12). Culture supernatants were studied for MMP-9 activity in gelatin zymography. The activities were quantified on a FluorChem using software AlphaEase (Alpha Innotech, San Leandro, CA). In a cell migration assay, RAW264.7 cells (5×10^4) suspended in serum-free DMEM and preincubated with the mAbs were applied to the upper chamber of fibronectin (FN)-precoated Transwells. DMEM containing 10% FBS was added to the lower chamber. After 4 h, cells migrating to the lower surface were counted with Diff-Quick stain (International Reagents, Hyogo, Japan). For siRNA transfection, RAW264.7 cells were transfected with mixture siRNAs against mouse CD9 or CD81 (B-Bridge International, Sunnyvale, CA) or control mixture RNAs (B-Bridge International) using Lipofectamine 2000 (Invitrogen). Gene silencing effects were confirmed by immunoblotting. The cells were cultured for 24 h in serum-free DMEM, and the culture supernatants were studied for MMP-9 activity by gelatin zymography.

Mice—The generation of CD9/CD81 DKO mice was described previously (13). These mice were backcrossed into the C57BL/6J background. The genotyping of littermates was achieved by PCR analysis. All animal experiments were performed with age- and sex-matched littermate controls using at least three animals at each time point. The mice were maintained in a specific pathogen-free facility, and all animal procedures were performed in accordance with the Osaka University guidelines on Animal Care.

Histology and Histomorphometric Analysis of the Lung—Lungs were inflated to 25 cm of water pressure with 10% buffered neutral formalin via an intratracheal cannula and embedded in paraffin. Parasagittal 5-μm-thick sections were stained with hematoxylin and eosin. Elastica-van Gieson stain for elastin, Masson's trichrome stain for collagen, and Alcian blue/periodic acid-Schiff (PAS) stain for mucus-secreting cells were also performed. Airspace size was quantified by calculating the mean chord length using the NIH Image software (14). Briefly, a minimum of 10 fields from each mouse lung was randomly acquired and visualized using the program Scion Image (Scion, Frederick, MD). The images were subject to sequential logical image match and operations with a horizontal and vertical grid. At least 200 measurements per field were made, and the length of the lines overlying airspace was averaged as the mean chord length.

Bronchoalveolar Lavage and Gelatin Zymography—Lungs of anesthetized mice were subjected to lavage with 3 volumes of 1 ml of phosphate-buffered saline containing 0.1% bovine serum albumin. Collected cells in the BALF were centrifuged onto Cytospin slides and visualized by Diff-Quick stain. Total cell counts and their subsets were determined using a hemocytometer. The supernatants of BALF were concentrated 10-fold using Centricon 10 filtration units (Millipore, Bedford, MA). Samples containing an equal amount of protein were electrophoresed in 10% zymogram gelatin gels (NOVEX, Carlsbad, CA). Gels were washed twice in 2.5% Triton X-100, incubated for 24 h with 40 mM Tris/HCl (pH 7.5), 10 mM $CaCl_2$, and 1 μM $ZnCl_2$, and stained with Coomassie Blue. Gelatinolytic activities were quantified on a FluorChem using software AlphaEase. The identical gels were treated in the presence of 0.01 M EDTA in parallel, and metal dependence, which is characteristic of MMPs, was confirmed by disappearance of lytic bands.